KeAi

CHINESE ROOTS
GLOBAL IMPACT

#### Contents lists available at ScienceDirect

# Petroleum Science

journal homepage: www.keaipublishing.com/en/journals/petroleum-science



# Original Paper

# A new method for the rate of penetration prediction and control based on signal decomposition and causal inference



Yong-Dong Fan  $^{a, b}$ , Hui-Wen Pang  $^{a, b, c}$ , Yan Jin  $^{a, b, *}$ , Han Meng  $^a$ , Yun-Hu Lu  $^b$ , Hao-Dong Chen  $^d$ 

- <sup>a</sup> College of Artificial Intelligence, China University of Petroleum, Beijing, 102249, China
- <sup>b</sup> State Key Laboratory of Petroleum Resources and Prospecting, China University of Petroleum, Beijing, 102249, China
- <sup>c</sup> College of Science, China University of Petroleum, Beijing, 102249, China
- <sup>d</sup> China National Offshore Oil Corporation (China) Limited, Hainan Branch, Haikou, 570100, Hainan, China

#### ARTICLE INFO

#### Article history: Received 22 September 2024 Received in revised form 1 April 2025 Accepted 2 April 2025 Available online 4 April 2025

Edited by Jia-Jia Fei

Keywords: Rate of penetration Signal decomposition Causal inference Parameters regulation Machine learning

#### ABSTRACT

Offshore drilling costs are high, and the downhole environment is even more complex. Improving the rate of penetration (ROP) can effectively shorten offshore drilling cycles and improve economic benefits. It is difficult for the current ROP models to guarantee the prediction accuracy and the robustness of the models at the same time. To address the current issues, a new ROP prediction model was developed in this study, which considers ROP as a time series signal (ROP signal). The model is based on the time convolutional network (TCN) framework and integrates ensemble empirical modal decomposition (EEMD) and Bayesian network causal inference (BN), the model is named EEMD-BN-TCN. Within the proposed model, the EEMD decomposes the original ROP signal into multiple sets of sub-signals. The BN determines the causal relationship between the sub-signals and the key physical parameters (weight on bit and revolutions per minute) and carries out preliminary reconstruction of the sub-signals based on the causal relationship. The TCN predicts signals reconstructed by BN. When applying this model to an actual production well, the average absolute percentage error of the EEMD-BN-TCN prediction decreased from 18.4% with TCN to 9.2%. In addition, compared with other models, the EEMD-BN-TCN can improve the decomposition signal of ROP by regulating weight on bit and revolutions per minute, ultimately enhancing ROP.

© 2025 The Authors. Publishing services by Elsevier B.V. on behalf of KeAi Communications Co. Ltd. This is an open access article under the CC BY license (http://creativecommons.org/licenses/by/4.0/).

# 1. Introduction

Drilling is an important part of oil and gas extraction, and drilling can establish a flow channel for oil and gas from underground reservoirs to the surface (Gao et al., 2021; Qiu et al., 2023; Fan et al., 2025). The rate of penetration (ROP) is the main metric to measure the efficiency of drilling, and the higher the rate of penetration (ROP) is, the shorter the drilling time is, and the lower the drilling cost is (Chen et al., 2023; Pei et al., 2024). ROP prediction refers to predicting the unknown ROP of the next stage based on some known physical parameters and corresponding ROP. The accurate prediction of ROP is of great significance for oil and gas extraction. Drilling workers can adjust some relevant physical parameters

\* Corresponding author. E-mail address: jiny@cup.edu.cn (Y. Jin). based on the predicted results of ROP to improve ROP, thereby shortening drilling time and reducing drilling costs (Chen et al., 2023).

At the present stage, ROP prediction is mainly divided into empirical model-based prediction and data-driven prediction. Maurer (1962) obtained an ROP calculation model with physical parameters such as WOB and bit size as dependent variables through a combination of experiments and on-site production analysis. Subsequently, several scholars have also proposed ROP prediction models applicable to various scenarios based on existing physical models. These models are mainly obtained by considering some relevant physical parameters based on existing experience and specific experiments (Bingham, 1965; Bourgoyne and Young, 1974; Hareland et al., 2010; Liu et al., 2015). The parameters considered in the model are the ones with higher correlations with ROP, but it does not mean that only these parameters have higher correlations with ROP. Traditional empirical models have clear physical meaning and are convenient for parameter regulation to improve ROP, but due to the complexity of oil and gas underground

List of abbreviations

EEMD	Ensemble empirical mode decomposition
BN	Bayesian network
TCN	Temporal convolutional network
EMD	Empirical mode decomposition
EEMD-TCN	EEMD and TCN fusion model
EEMD-BN-TCN	EEMD, BN, and TCN fusion model
MAPE	Mean absolute percent error
MAE	Mean absolute error
SI	Signal importance
PE	Permutation entropy
AE	Approximate entropy
IMF	Intrinsic mode function
WOB	Weight on bit
RPM	Revolutions per minute
WOB-IMF	Reconstructed signals related to WOB
RPM-IMF	Reconstructed signals related to RPM
Other-IMF	Reconstructed signals related to other parameters
LSTM	Long short term memory neural network
RF	Random forest
SVR	Support vector regression
ANN	Artificial neural networks
GBDT	Gradient boosting decision trees

reservoirs and the limited consideration of parameters in empirical models, the calculation accuracy of these models for ROP is generally low.

With the development and application of artificial intelligence technology, several scholars have also established data-driven ROP prediction models (Husam et al., 2021; Osman et al., 2021; Pang et al., 2022; Gong et al., 2022; Gan et al., 2023). The data-driven ROP prediction models can be mainly divided into two categories. In the first category, conventional machine learning models are used to predict ROP, such as the ANN model, SVR model, etc. (Melvin et al., 2019; Brenjkar and Delijani, 2022; Ahmed et al., 2022). The first category of model is an application of existing single machine learning methods. In the second category, improved machine learning models are used to predict ROP, such as the optimization of the particle swarm algorithm for the BP neural network prediction model (Ahmad et al., 2020; Li et al., 2021; Gamal et al., 2022; Oyedere and Gray, 2020). The second category of model mainly involves integrating multiple traditional machinelearning models or improving the algorithm structure of the conventional machine-learning models. For example, the models are established by improving the structure of existing machine learning models for predicting ROP (Ahmad et al., 2022a, 2022b; Gan et al., 2023; Liu et al., 2023). Although the ROP prediction accuracy of data-driven models achieves better performance than traditional physical models, it is still difficult to ensure both prediction accuracy and robustness simultaneously.

ROP is a parameter that varies with the time the drill bit penetrates the formation, so ROP can be regarded as a time series signal. The high complexity of ROP signals is the main reason for their difficulty in prediction. Signal decomposition can reduce the complexity of the original signal, decompose the complex signal into multiple groups of data with low complexity and high regularity, and get the final prediction results by predicting each group of decomposed sub-signals, thus improving the prediction accuracy (Ouyang et al., 2020; Peng et al., 2020; Zhang et al., 2020; Sun et al., 2022). After long-term research by domestic and foreign scholars, a signal decomposition and prediction process has been formed, which includes decomposition, prediction, and reconstruction output (Wang et al., 2022a; Li et al., 2023). The signal decomposition model decomposes the original complex signal into multiple sets of simple sub-signals. The prediction model predicts each group of sub-signals. The reconstruction model mainly reconstructs the predicted results of sub-signals to obtain the final output.

Currently, signal decomposition prediction models are widely used in the fields of wind power, carbon emissions, etc. but have not been applied to the prediction of ROP (Hossain et al., 2023; Song et al., 2023).

The core algorithms of the signal decomposition prediction model are signal decomposition algorithms and signal prediction algorithms, so many studies have also improved and analyzed the above two aspects (Nadirgil, 2023; Wang et al., 2023; Zhang et al., 2023). For signal decomposition prediction, signal decomposition is a very important step, and signal decomposition methods can be divided into two categories, signal decomposition based on specific basis functions and adaptive signal decomposition (Jiang, 2016). Signal decomposition based on specific basis functions mainly includes wavelet transform, Fourier transforms, etc. (Zheng et al., 2019; Wang et al., 2020). This kind of signal decomposition needs to determine the basis function, and signal decomposition based on the basis function, but the signal distribution in the actual engineering is complex, and it is difficult to find a suitable basis function. Since adaptive signal decomposition does not need to give the basis function in advance, it is completely based on the signal's characteristics, so it is widely used in engineering applications (Evangelidis and Kugiumtzis, 2023; Guo et al., 2023; Musluoglu and Bertrand, 2023). Empirical modal decomposition (EMD) is an adaptive signal decomposition method that is very suitable for the decomposition of non-smooth and nonlinear signals, but the signal is prone to modal aliasing after the decomposition of this method (Huang et al., 1998). Wu and Huang (2009) proposed the EEMD signal decomposition to address the shortcomings of the EMD, and this decomposition method has been widely used in later engineering practice. The combination of signal decomposition and machine learning models can effectively improve the prediction accuracy of time series data, and the robustness of the model is also enhanced. But there are many sub-signals after decomposition, and the prediction error of each group of sub-signals will lead to an increase in the final prediction error to a certain extent, and each group of sub-signals after decomposition does not have a certain mapping relationship with the actual physical parameters.

Aiming at the shortcomings of the above ROP prediction and signal decomposition prediction models, a new ROP prediction model was developed in this study, which is based on the time convolutional network (TCN) framework and integrates EEMD and BN causal inference. The model is named EEMD-BN-TCN. The model decomposes the ROP signal through EEMD and judges the causal relationships between the decomposed sub-signals and some important physical parameters based on BN. The model reconstructs the decomposed sub-signals into three groups based on causal relationships and predicts the three groups of signals based on TCN modeling to obtain the final ROP prediction results. Compared with other ROP prediction models, this model takes into account the influence of the sub-signals on the prediction error to reduce overall prediction error. Moreover, the EEMD-BN-TCN gives the corresponding relationship between the decomposed signal and the physical parameters, which can be used to regulate the important physical parameters to improve the ROP in practical applications.

## 2. Methodology

The main purpose of this study is to propose an improved TCN model (EEMD-BN-TCN) based on EEMD and BN causal inference, which combines the physical significance of correlated signals during signal processing and can be used for the prediction of important parameters in a variety of industrial fields. The EEMD-BN-TCN is here applied to the prediction of ROP in the process of oil and gas extraction. The research idea mainly includes data

collection and processing, modeling, and evaluation of results (Fig. 1). Data collection and processing include engineering data collection, data sampling alignment, outlier handling, missing value handling, data statistical analysis, and feature selection. The model establishment mainly introduces the EEMD-BN-TCN prediction model proposed in this study, which includes EEMD signal decomposition, BN causal inference, EEMD-BN signal preliminary reconstruction, and TCN signal prediction. The EEMD-BN-TCN model first decomposes a single predicted signal into multiple sets of predicted sub-signals using the EEMD method. Compared with the original signal, the decomposed sub-signals have lower complexity and stronger regularity, which is more conducive to the prediction model learning laws for prediction. In addition, considering that some human-controlled parameters often need to be reasonably regulated according to the prediction model in engineering applications, the EEMD-BN-TCN analyzes the causal relationship between the sub-signals and the physical parameters based on the BN causal inference and preliminary reconstructs the sub-signals based on the causal relationship. The preliminary reconstructed signals are categorized into signals affected by specific physical parameters and signals not affected by specific physical parameters. Finally, based on the TCN model, several groups of signals reconstructed are predicted separately. In practical applications, the changes of the signals affected by specific physical parameters can be observed according to the regulation of the specific physical parameters, to derive the change rule of the overall signals. After completing the decomposition prediction of the ROP signal, it is necessary to conduct a reasonable evaluation of the decomposition and prediction results. The evaluation of the results includes the evaluation of the signal complexity, and the evaluation of the prediction model, in which the evaluation of the prediction results is divided into the evaluation of the overall error and the evaluation of the relationship between the decomposed signal characteristics and the error.

## 2.1. Research background and dataset

#### 2.1.1. Research background

Drilling is an important part of oil and gas extraction, which can build the flow channel between underground oil and gas reservoirs and the surface. In the drilling process, ROP is the main metric to measure the drilling efficiency, and ROP affects the drilling cycle and drilling cost, so it is crucial to improve ROP according to the prediction model. Oil and gas reservoirs are often located thousands of meters underground, and to extract oil and gas, it is necessary to break the rocks covering the oil and gas reservoirs (Yan

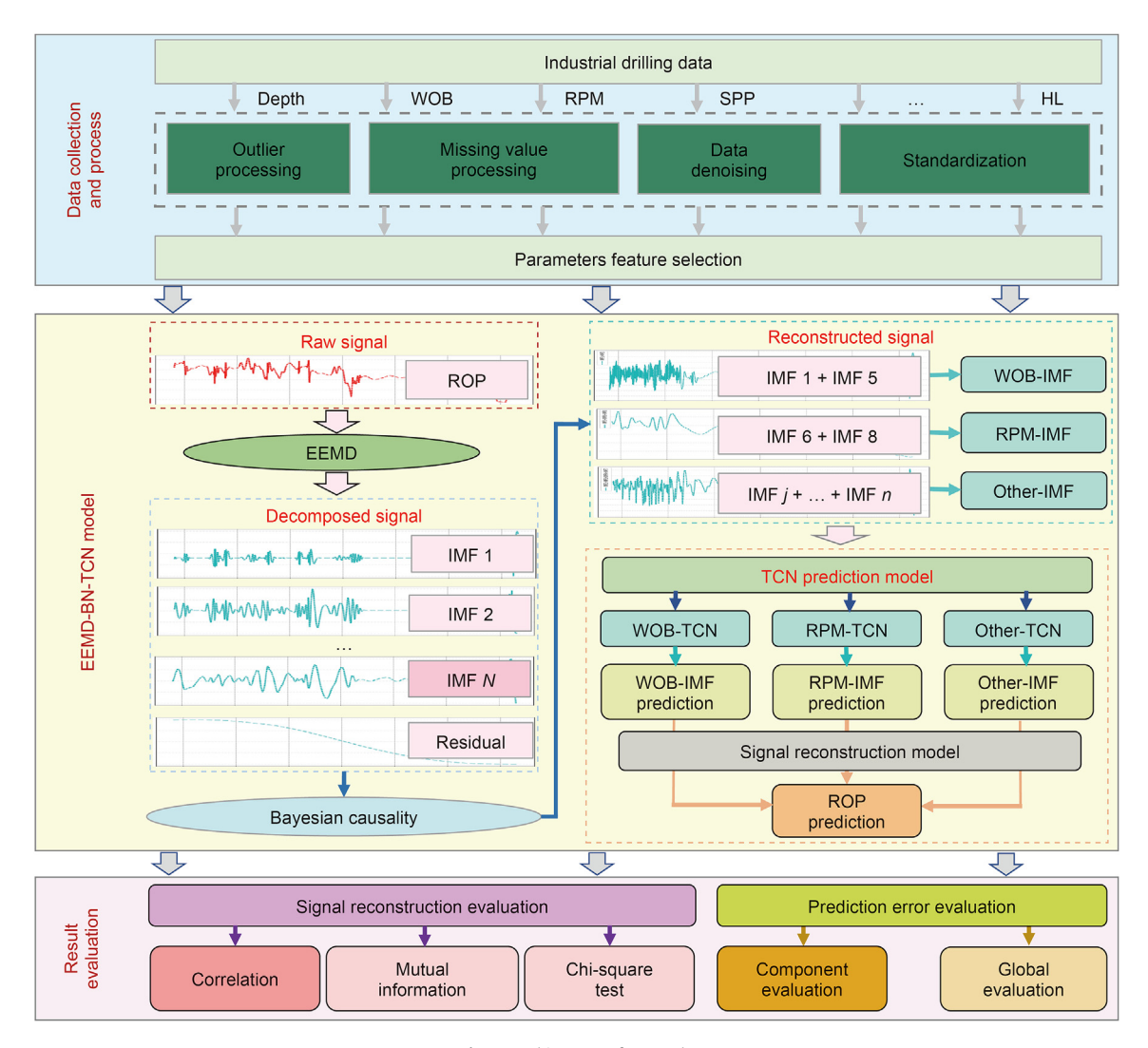


Fig. 1. Architecture of research.

et al., 2024). During breaking rocks, pressure is applied to the drill bit, and the drill string connected to the drill bit drives the drill bit to rotate, thereby breaking the rock (Fig. 2). In this process, the revolutions per minute (RPM) of the drill string and the weight of bit (WOB) are the key factors affecting the ROP, and RPM and WOB are parameters that can be controlled by well-drilling workers. Therefore, if the sub-signals affected by WOB and RPM can be separated from the original ROP signal, it will reduce the difficulty of predicting and improving ROP.

## 2.1.2. Data collection and processing

The drilling data obtained from the engineering project is very complicated, and the sampling interval, sampling range, and data accuracy of different parameters are often very different. In addition, some of the data recorded in the engineering project may have abnormal values and missing values. Therefore, it is necessary to carry out a series of processing of the data obtained from the project. Moreover, due to the factors of the collection environment and collection equipment, there are noise values in the collected data. This study applies wavelet filtering denoising technology to denoise the collected data. This study focuses on 3273 pieces of data from an offshore oil well. These data have obvious temporal characteristics. The distribution range and meaning of different parameters after data preprocessing are shown in Table 1.

After completing the preprocessing of the data, feature selection is required. Feature selection is based on Pearson correlation analysis, Spearman correlation analysis, and gradient boosting decision tree (GBDT) to select physical parameters with high correlation to ROP. GBDT is used for feature selection by gradually reducing feature parameters to predict ROP. If the prediction error increases significantly after removing a specific feature parameter, that feature is considered to have a high correlation with ROP. In the prediction process, GBDT uses the mean absolute percentage error (MAPE) as the prediction error metric (Fig. 3(b)). Through analysis, it is finally concluded that the large hook load (HL) and bit size (BS) have low correlations with ROP, and the eight groups of parameters, namely, Depth, WOB, RPM, SPP, T, Mw, Flow, and Tor have high correlations with ROP, so the subsequent study is mainly centered on the above parameters (Fig. 3).

Among these parameters, WOB and RPM are two groups of parameters that are easy to be regulated by the staff during drilling, and they are also two groups of parameters with high correlations with ROP (Fig. 3). Therefore, if the parts affected by WOB and RPM can be separated from the complex ROP signal and the prediction models can be established separately, it will be beneficial to

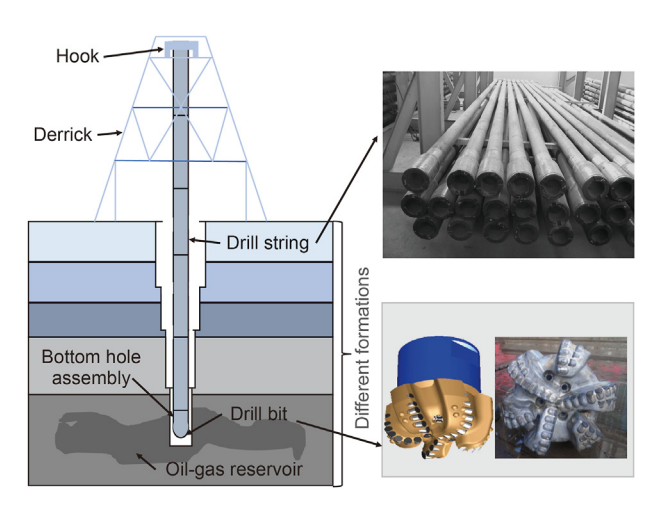


Fig. 2. Drilling process diagram.

**Table 1** Distribution of key parameters.

Symbol	Meaning	Unit	Minimum	Maximum
Depth	Vertical depth	m	2154	3669
WOB	Weight on bit	ton	1.51	19.45
RPM	Revolutions per minute	r/min	60	106
SPP	Stand pipe pressure	MPa	10.23	30.37
T	Temperature out	°C	19.2	27.5
Mw	Density out	g/cm <sup>3</sup>	1.23	1.45
Flow	Flow	L/min	3676	5140
Tor	Torque	N⋅m	5342	47670
ROP	Rate of penetration	m/h	18.6	92.7

rationally regulate WOB and RPM in real-time when drilling, thus improving the overall efficiency.

#### 2.2. Signal decomposition and reconstruction model

The EEMD model decomposes the original complex and irregular ROP signal into multiple sub-signals with low complexity and high regularity. The decomposed sub-signals make it easier for the TCN model to learn the intrinsic physical laws from them. If each group of sub-signals is predicted individually by TCN models, it will face three insurmountable problems: the overall error reduction is not significant, the computation takes longer, and the sub-signals lack physical significance. When sub-signals are predicted separately, the prediction error of each group of sub-signals will be accumulated into the final prediction error. Although the overall prediction error may be reduced compared to directly predicting the ROP signal through the TCN model, the error reduction is not significant. The prediction of each group of sub-signals consumes computational resources and time, so the overall computation time increases significantly. The decomposed sub-signals lack actual physical meaning, which makes it impossible to adjust specific engineering parameters according to the engineering requirements in combination with the prediction model. To solve the above three problems, this section determines the causal relationship between the sub-signals and specific physical parameters based on BN causal inference and initially reconstructs the sub-signals based on the causal relationship. Therefore, this section mainly includes EEMD signal decomposition and EEMD-BN signal reconstruction.

# 2.2.1. Signal decomposition

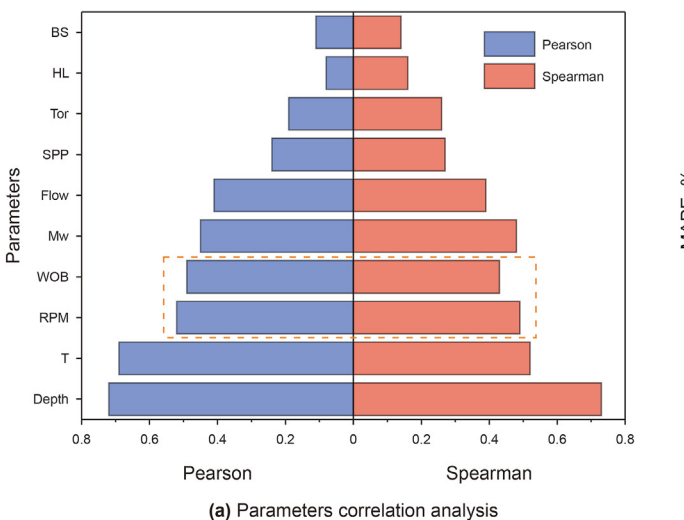
In EEMD signal decomposition, the original signal is first added with an equal-length white noise signal (Eq. (1)), and the EEMD decomposition is carried out for the new signal. The new signal is decomposed into multiple intrinsic mode function signals (IMF) and a residual signal (Eq. (2)). The above process needs to be repeated several times until the residual signal even after decomposition no longer satisfies the decomposition conditions. The resulting IMF signals and the residual signal are summed to the original signal (Eq. (3)). The IMF signals and residual signal can be collectively referred to as sub-signals of the original signal.

$$x_i(t) = x(t) + n_i(t) \tag{1}$$

$$x_{i}(t) = \sum_{j=1}^{J} C_{i,j}(t) + r_{i}(t)$$
 (2)

$$x(t) = \sum_{j=1}^{J} C_j(t) + r(t)$$
 (3)

where x(t) is the original signal,  $n_i(t)$  is a noise sequence,  $x_i(t)$  is the



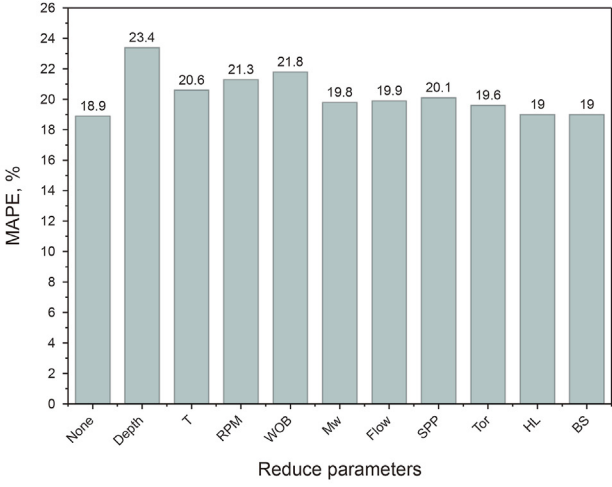


Fig. 3. Feature selection.

signal sequence after the addition of white noise,  $C_{i,j}(t)$  is the IMF signal decomposed, and  $r_i(t)$  is the residual signal, x(t) is the original signal,  $C_j(t)$  is the IMF signal decomposed in the final decomposition result, and r(t) the residual signal remaining in the final decomposition result.

## 2.2.2. Signal reconstruction

Signal reconstruction first needs to determine the causal relationship between sub-signals and specific physical parameters (WOB and RPM) based on the BN causal inference, and then initially reconstruct sub-signals based on the causal relationship and the inverse principle of EEMD decomposition. The BN is formulated as  $B = \langle \mathcal{G}, \theta \rangle$  where  $\mathcal{G} = \langle V, E \rangle$ , V denotes the variables, E describes the relationship between the variables and  $\theta$  quantitatively describes the relationship between the variables. The  $B = \langle \mathcal{G}, \theta \rangle$ is a representation of causal dependencies between variables  $X_1, X_2, ..., X_T$  by means of a directed acyclic graph (DAG) (Wang et al., 2022b; Valverde et al., 2023; Chen et al., 2022). For variable  $X_i$ , if  $X_j$  and  $X_k$  are its parent nodes ( $X_j$  and  $X_k$  are the cause variables of  $X_i$ ), and  $X_i$  and  $X_k$  are denoted as the set  $Z_i^B$ . The  $Z_i^B$  is the set consisting of all the parent nodes of  $X_i$  in B, then the conditional probability of  $\theta$  can be expressed as Eq. (4). Combining the independence relation and conditional probability of the BN, then the joint probability distribution can be expressed as Eq. (5).

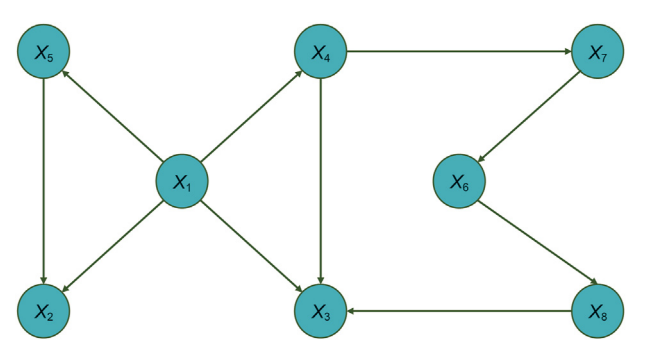


Fig. 4. Bayesian network causal relationship diagram.

$$\theta_{X_i|Z^B} = P_B(X_i|Z_i^B) \tag{4}$$

(b) GBDT prediction error

$$P(X_1, X_2, ..., X_T) = \sum_{i=1}^{T} P(X_i | Z_i^B)$$
 (5)

Taking Fig. 4 as an example, there are 8 nodes in the graph, the BN of this graph can be expressed as Eqs. (6)–(8), and the joint probability distribution can be expressed as Eq. (9) according to the BN. Eq. (6) represents the set of 8 nodes in the graph structure. Eq. (7) represents the causal relationships among the 8 nodes, where  $X_1 \rightarrow X_2$  indicates that  $X_1$  is a causal factor influencing changes in  $X_2$ . Eq. (8) represents the set of conditional probabilities for the causal relationships among the 8 node variables. For example,  $P(X_2|X_1,X_5)$  denotes the conditional probability of  $X_2$  given the causal parameters  $X_1$  and  $X_5$ . Eq. (9) represents the joint probability distribution of the 8 nodes.

$$V = \{X_1, X_2, X_3, X_4, X_5, X_6, X_7, X_8\}$$
 (6)

$$E = \{X_1 \to X_2, X_1 \to X_3, \dots, X_8 \to X_3\}$$
 (7)

$$\theta = \{P(X_1), P(X_2|X_1, X_5), P(X_3|X_1, X_4, X_8), P(X_4|X_1), P(X_5|X_1), \\ P(X_6|X_7), P(X_7|X_4), P(X_8|X_6)\}$$
 (8)

$$P(X_1, X_2, ..., X_8) = P(X_1)P(X_2|X_1, X_5)P(X_3|X_1, X_4, X_8)...P(X_8|X_6)$$
(9)

Substituting the component  $C_j(t)$  and residual r(t) after EEMD decomposition in Eq. (3) into Eq. (6), and substituting the physical parameters WOB, RPM into Eq. (6) as well, the BN model node variable set composed of sub-signals and physical parameters can be represented as Eq. (10), where  $C_1(t), \ldots, X_{WOB}, X_{RPM}$  are nodes in the DAG structure. The causal relationship between the variables can be expressed as Eq. (11), where  $X_{WOB} \rightarrow C_1(t)$  indicates that WOB is a causal parameter of the sub-signal  $C_1(t)$ . In the variable relationship, this study focuses on the relationship between the decomposed sub-signal and the physical parameters WOB, RPM. The causal relationship is substituted into Eq. (3) based on Eq. (11) to obtain three reconstructed signals of the sub-signals after EEMD

decomposition (Eqs. (12)—(14)). For example, Eq. (12) indicates that WOB is the causal parameter for  $C_1(t)$  and  $C_2(t)$ . Therefore, according to the EEMD signal decomposition principle,  $C_1(t)$  and  $C_2(t)$  are summed to obtain WOB-IMF. To prevent signal aliasing, each sub-signal decomposed by EEMD can only appear in one of the WOB-IMF, RPM-IMF, or Other-IMF groups. If a sub-signal appears in the WOB-IMF group, it cannot appear in the other two groups. If a sub-signal has causal relationships with both WOB and RPM, its correlation with WOB and RPM is calculated, and it is assigned to the group with the stronger correlation.

$$V = \{C_1(t), C_2(t), ..., C_I(t), r(t), X_{WOB}, X_{RPM}\}$$
(10)

$$E = \{X_{WOB} \to C_1(t), X_{WOB} \to C_2(t), ..., C_2(t) \to C_4(t), ...\}$$
 (11)

$$WOB-IMF = C_1(t) + C_2(t)$$
(12)

RPM-IMF = 
$$C_3(t) + C_4(t) + r(t)$$
 (13)

Other-IMF = 
$$\sum_{i=5}^{J} C_j(t)$$
 (14)

#### 2.3. EEMD-BN-TCN model

Through the signal decomposition of EEMD and the preliminary reconstruction of the signal, the ROP signal is decomposed and reconstructed into three groups, namely, RPM-IMF, WOB-IMF, and Other-IMF. In the ROP prediction modeling, the RPM-IMF, WOB-IMF, and Other-IMF are predicted separately, and the prediction results of RPM-IMF, WOB-IMF, and Other-IMF are reconstructed by EEMD model to get the final prediction results of ROP. Both the original ROP, WOB-IMF, RPM-IMF, and Other-IMF are signals with strong temporal sequences, so it is necessary to choose a model that can effectively deal with the time series data when selecting the base model for prediction. TCN takes advantages of the time series data processing method and the convolutional neural network, and it has an outstanding advantage in the prediction of the time series data (Bai et al., 2018). Therefore, the TCN is finally selected in this study as the base prediction model.

TCN is a convolutional network model that can be used for time series prediction (Bai et al., 2018; Yang et al., 2023). TCN mainly includes causal convolution, dilated convolution, and residual block (Fig. 5), which can effectively solve the prediction problem of multivariate complex time series. The causal convolution based on the conventional convolution operation excludes the influence of future information on the current output to meet the requirements of time series data. Conventional convolution ignores the time sequence of data, and the output information in conventional convolution is not only related to the past information but also affected by the future information. For time series data, future information is not known at the current moment, so the current output depends only on the past input (Eq. (15), Fig. 5). Although causal convolution takes into account the time sequence of data, its perceptual domain becomes smaller compared to conventional convolution. To solve the problem of a limited perceptual domain, dilated convolution is introduced in the TCN model. Dilated convolution increases the perceptual domain by interval sampling the input. When the dilation factor is equal to 1 (d = 1), it indicates that each piece of information of the input needs to be sampled. When the dilation factor is equal to 2, the input is sampled at a sampling interval of 2. When the dilation factor is equal to n, the

input is sampled at sampling interval of n (Fig. 5). For the sequence  $X = \{X_1, X_2, ..., X_T\}$  and the convolution kernel f, the corresponding dilated convolution operation can be expressed as Eq. (16). For the TCN model, the network depth will directly affect the network on the extraction of features. Deeper convolutional network layers can enhance the performance of the TCN model, but too many network layers can also lead to an increase in both the time and spatial complexity of the network. In addition, complex network layers may also cause gradient explosions or vanishing gradients. The residual block can solve these problems to a certain extent (He et al., 2015). The residual block in TCN consists of two sets of causal convolution layers, two sets of dilated convolution layers, two sets of weights normalization layers, two sets of activation function layers, and a dropout layer (Fig. 5).

For the EEMD-BN-TCN model, it is necessary to build a prediction model based on the labels WOB-IMF, RPM-IMF, and Other-IMF with the corresponding feature parameters, respectively, and finally get the prediction results  $\tilde{y}_{\text{WOB-IMF}}$ ,  $\tilde{y}_{\text{RPM-IMF}}$ , and  $\tilde{y}_{\text{Other-IMF}}$ . Substitute the above three sets of prediction results into Eq. (3) to obtain the final prediction results  $\tilde{y}$  (Eq. (17)).

$$\tilde{y}_t = f(X_1, X_2, X_3, ..., X_{t-1})$$
 (15)

$$F(T) = \sum_{i=0}^{k-1} f(i) \cdot X_{T-d \cdot i}$$
 (16)

$$\overset{\sim}{y} = \overset{\sim}{y}_{\text{WOR-IMF}} + \overset{\sim}{y}_{\text{RPM-IMF}} + \overset{\sim}{y}_{\text{Other-IMF}}$$
 (17)

where  $\tilde{y}_t$  is the output at moment t,  $X_{t-1}$  is the parameter containing the feature information at moment t-1, f is the optimal model obtained by fitting, F is the dilated convolution function of X, d is the dilated factor, k is the filter size,  $T-d\cdot i$  accounts for the direction of the past.

# 2.4. Model evaluation

The model evaluation includes the evaluation of sub-signal complexity and the evaluation of prediction results. The evaluation of sub-signal complexity includes the evaluation of signal complexity after EEMD decomposition and the evaluation of the relationship between the key physical parameters and the restructured sub-signals. The assessment of prediction results mainly evaluates the prediction results of different models and the impact of different decomposed sub-signal prediction errors on the overall prediction errors.

#### 2.4.1. Signal complexity evaluation

For machine learning models, the lower the signal complexity. the better it is for the model to learn its intrinsic laws, so the complexity of the EEMD decomposed signal needs to be lower than the complexity of the original ROP signal. The signal reconstruction is to reconstruct the signals affected by WOB into WOB-IMF and the signals affected by RPM into RPM-IMF. So it is necessary to ensure that the complexity of WOB-IMF, RPM-IMF, and Other-IMF is lower than the complexity of the original ROP signal. Signal complexity assessment is performed based on the permutation entropy and approximate entropy. Permutation entropy is used to calculate the complexity of the sequence by reordering the vectors in the phase space through phase space reconstruction of the sequence (Eq. (18) and Eq. (19)). Approximate entropy has more stable quantization results for non-smooth and non-linear sequences, and the calculation of approximate entropy is mainly done by Eq. (20) and Eq. (21).

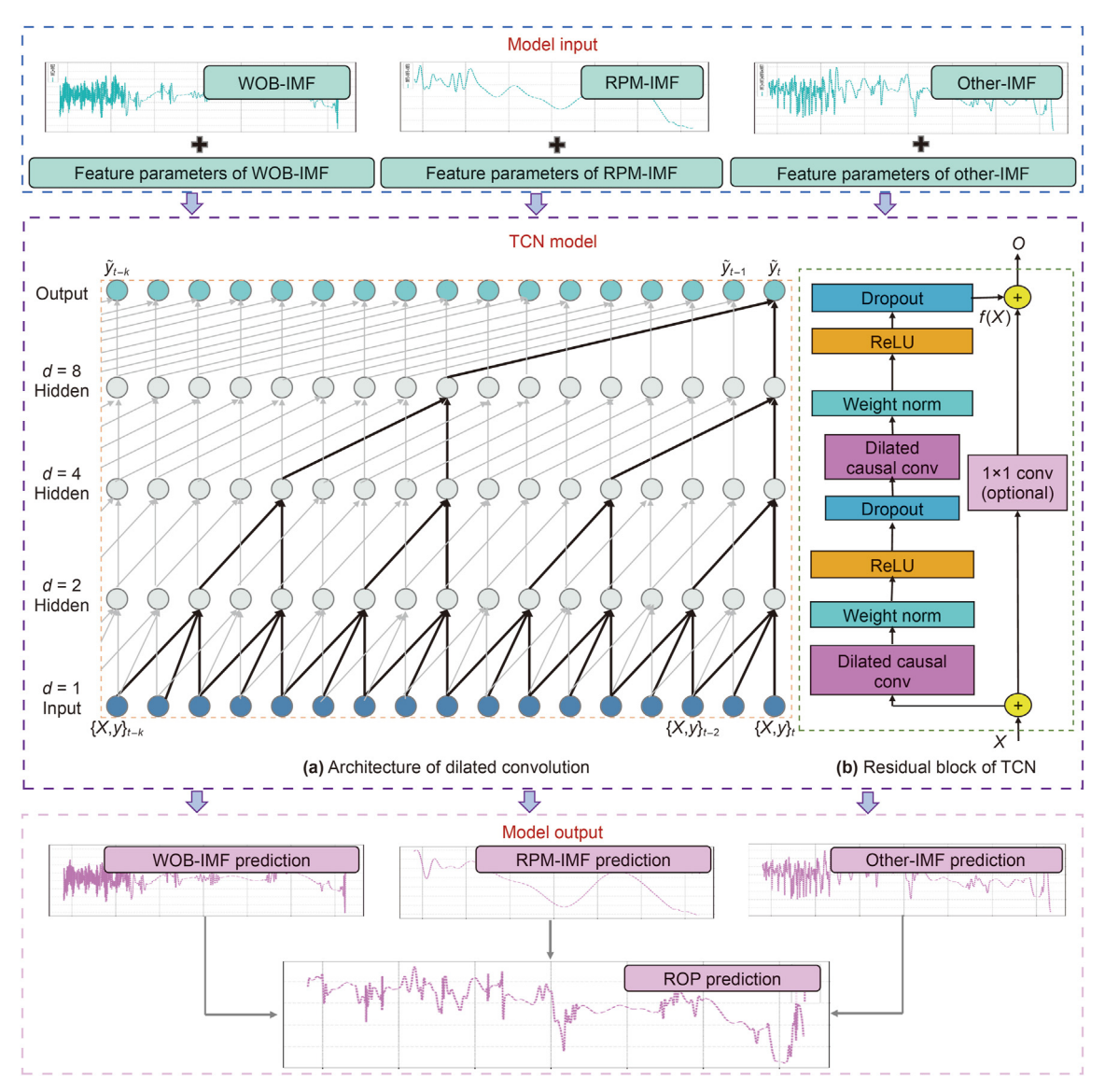


Fig. 5. TCN prediction process.

$$H_{PE}(m) = -\sum_{k=1}^{m!} p(\pi_k) \log p(\pi_k)$$
 (18)

$$p(\pi_k) = \frac{\sum\limits_{k=1}^{N-m+1} \{\pi_k\}}{m!(N-m+1)} \tag{19}$$

$$ApEn(M,r) = \varnothing^{M}(r) - \varnothing^{M+1}(r)$$
(20)

$$\emptyset(r) = \frac{\sum_{i=1}^{N-M+1} \ln C_i^M(r)}{N-M+1}$$
 (21)

where  $H_{PE}(m)$  is permutation entropy, m is the embedding dimension (generally taken as 3–7),  $p(\pi_k)$  is the probability corresponding to one of the permutations, N is the length of the sequence, ApEn(M,r) is the approximation entropy, M is the input dimension (generally taken as 1 or 2), r is the threshold value, and

 $C_i^M(r)$  is the sequence distance function.

After decomposition and reconstruction, the complexity of all sub-signals must be lower than that of the original ROP signal. In addition, it is necessary to verify whether the relationship between the reconstructed signal and physical parameters is reasonable. For the reconstructed signals, it is necessary to ensure that WOB is only related to WOB-IMF and RPM is only related to RPM-IMF. The above relationships are mainly tested through the correlation coefficient, mutual information test, and chi-square test.

#### 2.4.2. Prediction error evaluation

The error assessment includes the overall prediction errors and the contribution of individual sub-signal prediction errors to the overall errors. The error analysis is performed based on the mean absolute percentage error (MAPE) and  $R^2$  (Eq. (22) and Eq. (26)). To evaluate the relationship between the prediction errors of subsignals and the overall prediction errors, this study introduced the mean absolute error of sub-signal prediction results and the mean absolute error of the overall prediction results (Eqs. (23)–(25)).

$$MAPE = \frac{1}{n} \sum_{i=1}^{n} \left| \frac{\tilde{y}_i - y_i}{y_i} \right|$$
 (22)

$$MAE_{j} = \frac{1}{n} \sum_{i=1}^{n} |\tilde{y}_{i,j} - y_{i,j}|$$
 (23)

MAES = 
$$\sum_{j=1}^{m} MAE_j = \frac{1}{n} \sum_{j=1}^{m} \sum_{i=1}^{n} |\tilde{y}_{i,j} - y_{i,j}|$$
 (24)

MAE = 
$$\frac{1}{n} \sum_{i=1}^{n} \left| \sum_{j=1}^{m} \tilde{y}_{i,j} - \sum_{j=1}^{m} y_{i,j} \right|$$
 (25)

$$R^{2} = 1 - \frac{\sum_{i=1}^{n} (\tilde{y}_{i} - y_{i})^{2}}{\sum_{i=1}^{n} (\bar{y}_{i} - y_{i})^{2}}$$
 (26)

where MAPE is the mean absolute percentage error,  $\tilde{y}_i$  is the predicted value of data point  $i, y_i$  is the true value of data point i, n is the total number of data points, MAE $_j$  is the mean absolute error of the sub-signal j,  $\tilde{y}_{i,j}$  is the predicted value of the sub-signal j at the data point  $i, y_{i,j}$  is the true value of the sub-signal j at the data point i, MAES is the sum of the mean absolute errors for all the sub-signals, and MAE is the mean absolute error of final ROP prediction results.

## 3. Results

This section focuses on the decomposition of the raw ROP by EEMD (Section 3.1), the reconstruction of the signal based on the EEMD-BN (Section 3.2), the analysis of the prediction results of different models (Section 3.3), and the analysis of the effect of the decomposed sub-signals on the prediction error (Section 3.4).

For the TCN model and the improved TCN models, hyperparameters directly affect the prediction accuracy of the model. In determining the hyperparameters of the TCN model, this study employed the particle swarm optimization (PSO) algorithm to optimize the hyperparameters and obtain the best set of parameters. The PSO optimizes TCN hyperparameters by initializing a swarm of particles, each representing a set of hyperparameters. The algorithm evaluates their performance based on a defined objective function, updates the particles' positions and velocities, and iterates to find the best hyperparameters that minimize the validation loss. Additionally, considering limited computational resources and the large number of sub-models, after the PSO algorithm provides the corresponding hyperparameter combinations, some hyperparameters were manually adjusted with minimal impact on prediction accuracy to improve computational efficiency. The main hyperparameters of the TCN-related models involved in this study are shown in Table 2.

## 3.1. Signal decomposition based on EEMD

The EEMD decomposes the original signal into several IMF signals and a residual signal. Compared with the original signal, the regularity of the decomposed signal is more obvious. Taking the data of an offshore oil well as an example, EEMD decomposes the original signal into seven IMF signals and a residual signal (Fig. 6). From the perspective of signal stationarity, the seven IMF signals

are all stationary signals and the residual signal is non-stationary signals, but the residual signal is a monotonically decreasing signal with well depth. The original ROP signal is neither a stationary signal nor a monotonic signal, so the regularity of the decomposed eight groups of sub-signals is enhanced (Fig. 6).

Fig. 6 shows that the regularity of the sub-signals is enhanced compared with the original signal. To further quantitatively analyze the difference between the sub-signals and the original signal, this study evaluates the complexity of the original ROP signal and the sub-signals by the permutation entropy (Eq. (18)) and the approximate entropy (Eq. (20)). The value of parameter m in Eq. (19) is crucial in the calculation of the arrangement entropy, and mis usually taken from 3 to 7. In the calculation of the approximate entropy, the main parameters are M and r. M is usually taken from 1 or 2 (Eq. (21)), and r is usually taken from 0.1 to 0.25. For the calculation of the permutation entropy, it is concluded that the permutation entropy of the original ROP is the highest regardless of the value of m, and the permutation entropy of the eight groups of sub-signals decreases in turn (Fig. 7(a)). For the approximate entropy, the value of approximate entropy and permutation entropy presents basically the same rule of change. The approximate entropy of the original ROP signal is the highest, and the approximate entropy of the sub-signals is gradually reduced (Fig. 7(b)). The complexity of the decomposed sub-signals is lower than the original signal, and the complexity of some sub-signals is much lower than the original signal, so it is relatively easy to apply the machine learning model to learn the intrinsic law of data from the subsignals for prediction. It can be seen that the idea of decomposition prediction of ROP signals by EEMD is feasible.

## 3.2. Signal reconstruction based on EEMD-BN

EEMD can decompose the ROP signal into seven IMF signals and a residual signal. If the eight sub-signals are modeled one by one, the computational time is long, and the prediction of each sub-signal has an error. The errors of each sub-signal will accumulate into the final error, so the individual prediction is not conducive to the reduction of the overall error. In addition, the eight sub-signals do not have a good mapping relationship with the physical parameters related to the ROP. Therefore, if the eight sub-signals are modeled directly, it is difficult to adjust the physical parameters according to the prediction models in the actual engineering applications.

In practical engineering applications, WOB and RPM are parameters that have a greater impact on ROP (Fig. 3), and the parameters are two groups of parameters that can be adjusted by drilling workers. So the eight sub-signals can be categorized into signals affected by WOB but not by RPM, signals affected by RPM but not by WOB, and signals affected neither by WOB nor by RPM. Bayesian causal inference combines Bayesian statistical laws with causal inference methods and has good results in practical applications. PCboot and Two-Stage are two typical Bayesian causal inference methods. Therefore, in determining the relationship between physical parameters and sub-signals, this study analyzes the causal relationship between sub-signals and WOB, and RPM by two Bayesian network causal inferences based on the PCboot and the Two-Stage. The causal relationships given by the two BN models are the same, both of which consider RPM as the cause parameter of IMF5 and IMF6, WOB as the cause parameter of IMF7 and residual, while the other four sub-signals have no causal relationship with WOB and RPM (Fig. 8). Therefore, based on the inverse principle of EEMD, IMF5 and IMF6 are reconstructed as RPM-IMF, IMF7 and residual are reconstructed as WOB-IMF, and IMF1, IMF2, IMF3, and IMF4 are reconstructed as Other-IMF (Fig. 9). IMF1, IMF2, IMF3, and IMF4 are short-period signals influenced by other engineering and

**Table 2** Hyperparameters of the prediction models.

Model	Convolutional kernel size	Number of kernels	Dilated factor	Input size	Output size
TCN	9	80	2	80	5
TCN-IMF1	11	75	2	60	5
TCN-IMF2	11	75	2	60	5
TCN-IMF3	11	75	2	60	5
TCN-IMF4	11	75	2	60	5
TCN-IMF5	9	70	2	50	10
TCN-IMF6	9	70	2	50	10
TCN-IMF7	7	30	2	50	10
TCN-Residual	7	20	2	60	20
TCN-WOB-IMF	9	40	2	80	20
TCN-RPM-IMF	7	40	2	70	10
TCN-Other-IMF	11	60	2	70	10

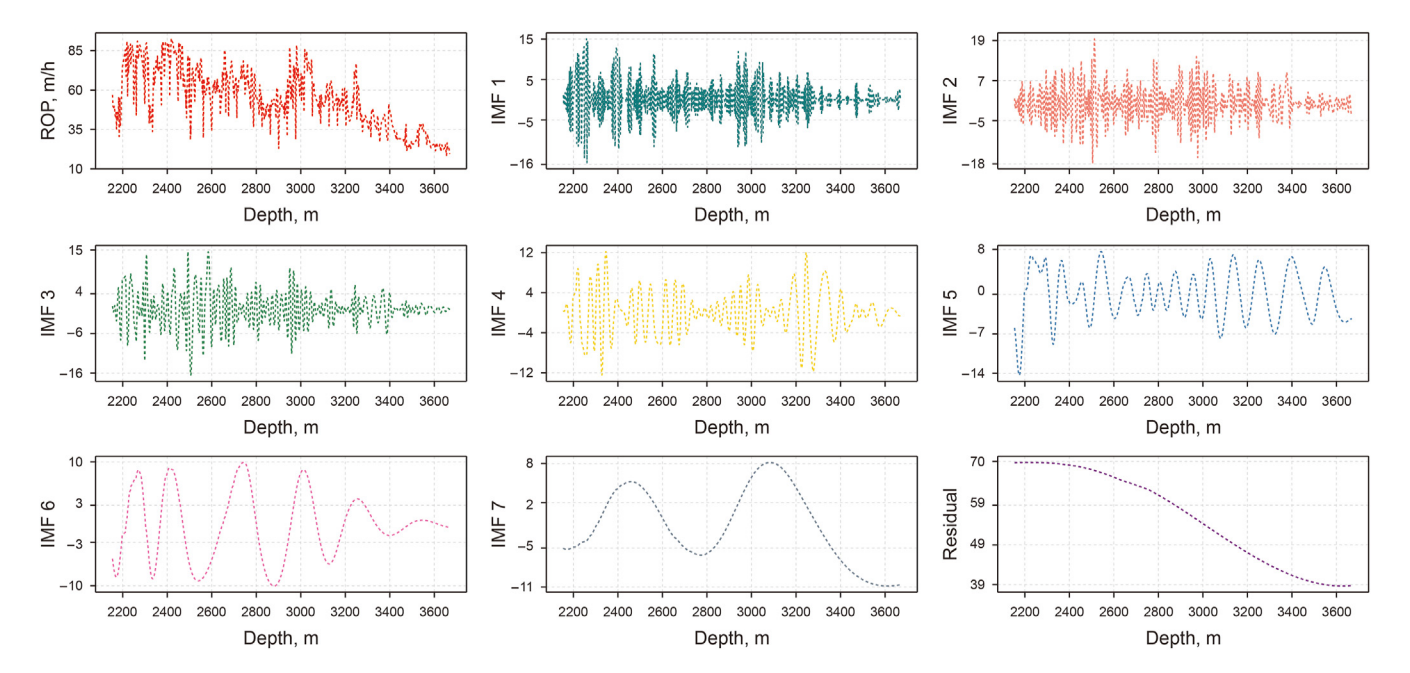


Fig. 6. The decomposed signals through EEMD.

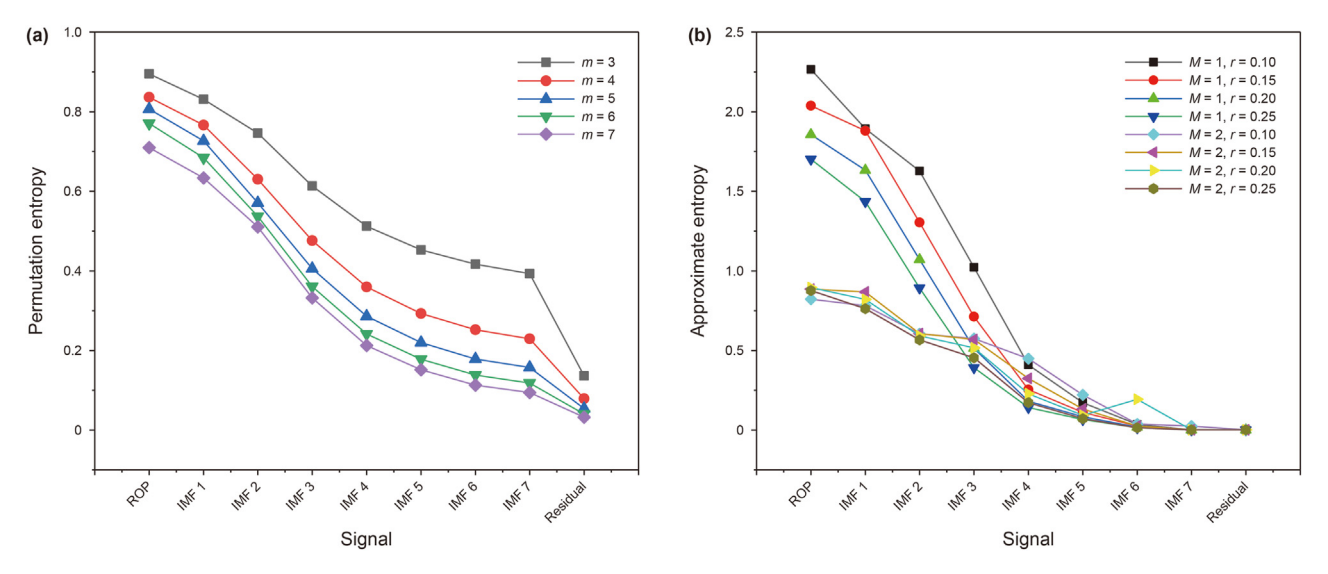


Fig. 7. Evaluation of signal complexity after EEMD decomposition.

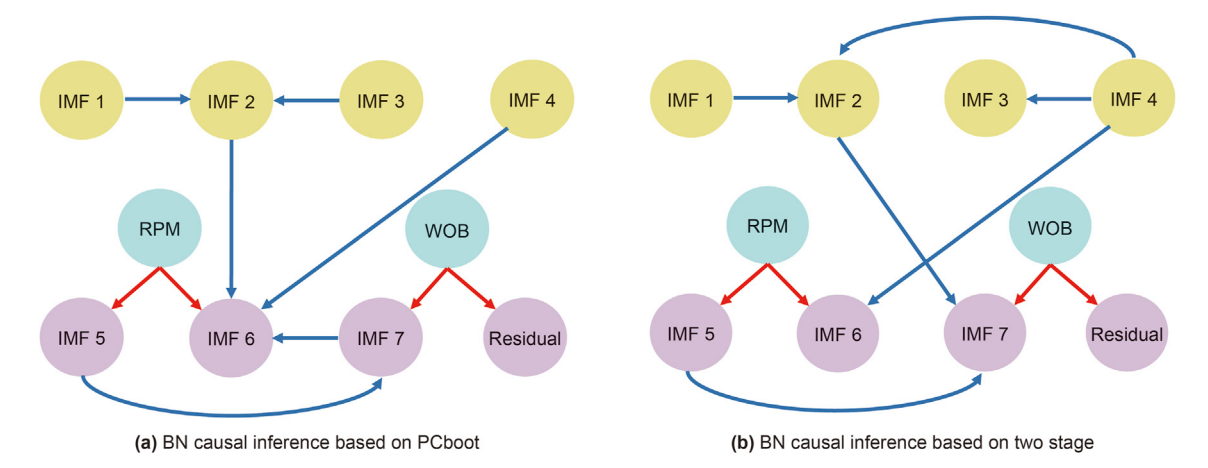


Fig. 8. Bayesian causal inference.

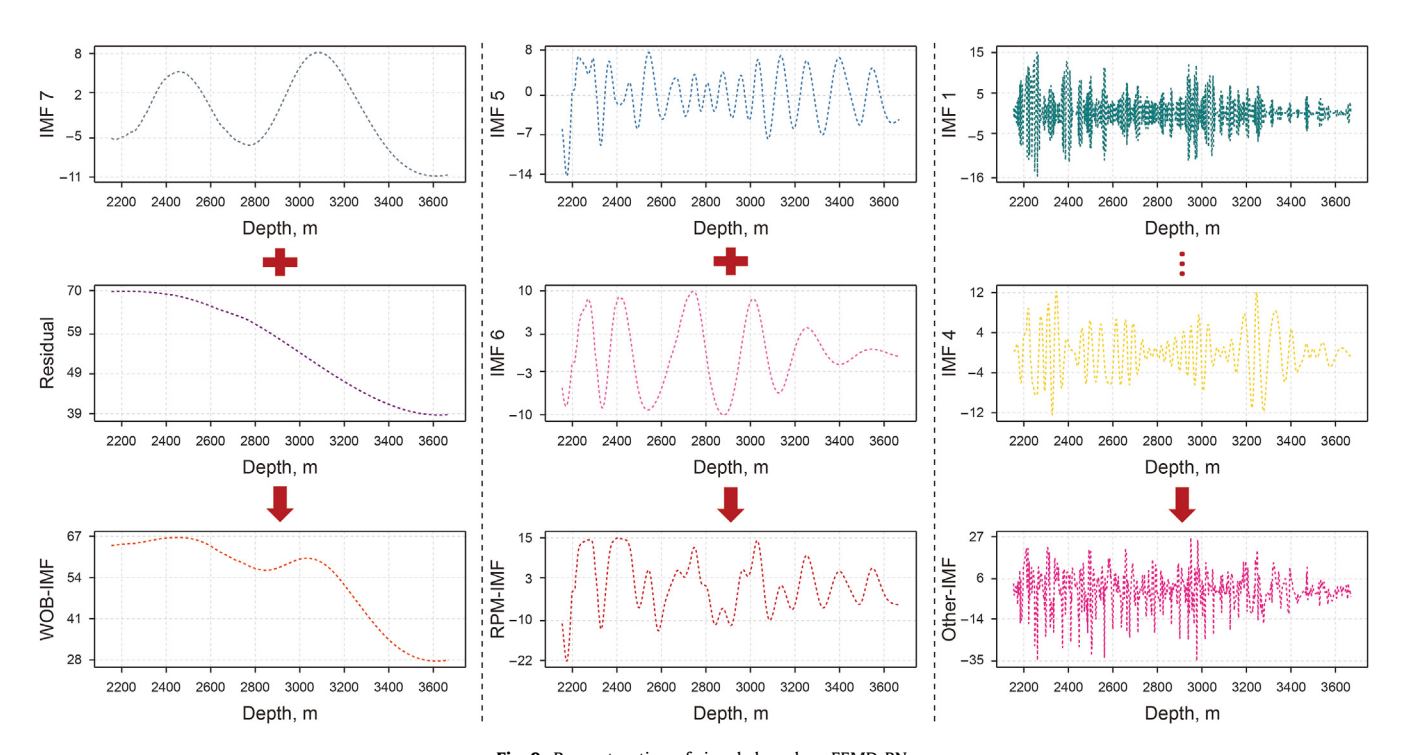


Fig. 9. Reconstruction of signals based on EEMD-BN.

geological factors, aside from WOB and RPM.

The reconstructed signals should satisfy two conditions. Firstly, WOB is only correlated with WOB-IMF, and RPM is only correlated with RPM-IMF. Secondly, the reconstructed three signals have lower complexity (lower permutation entropy and approximation entropy) compared with the original ROP signal. In the analysis of the correlation between the reconstructed signals and the corresponding physical parameters, the main assessments were made by correlation (Pearson correlation, Spearman correlation), mutual information, and chi-square test. The results of Pearson correlation and Spearman correlation analysis are the same, and it can be concluded that WOB shows strong correlation with WOB-IMF, while the absolute values of the correlation coefficients of WOB with RPM-IMF and Other-IMF are lower than 0.2, and it can be assumed that WOB is not correlated with RPM-IMF and Other-IMF (Fig. 10(a)). For RPM, the correlation coefficients between RPM and RPM-IMF are greater than 0.5, while the absolute values of the

correlation coefficients between RPM and WOB-IMF and Other-IMF are lower than 0.1 (Fig. 10(b)). The results of the mutual information test were consistent with the correlation test. The mutual information values of WOB and WOB-IMF were much higher than those of the other two groups, and the mutual information values of RPM and RPM-IMF were much higher than those of the other two groups (Fig. 10(c)). The P-value of WOB with WOB-IMF in the chi-square test is lower than 0.05, while the P-values with the other two groups of signals are higher than 0.2. Therefore, it can be considered that there is a high confidence that WOB is correlated with WOB-IMF, while there is a low confidence that WOB is correlated with the other two groups of signals. The results of the RPM chisquare test also indicate that RPM is very likely to be correlated with RPM-IMF (Fig. 10(d)). After comprehensive analysis, it can be finally determined that WOB is only correlated with WOB-IMF and not with the other two groups of signals, and RPM is only correlated with RPM-IMF and not with the other two groups of signals.

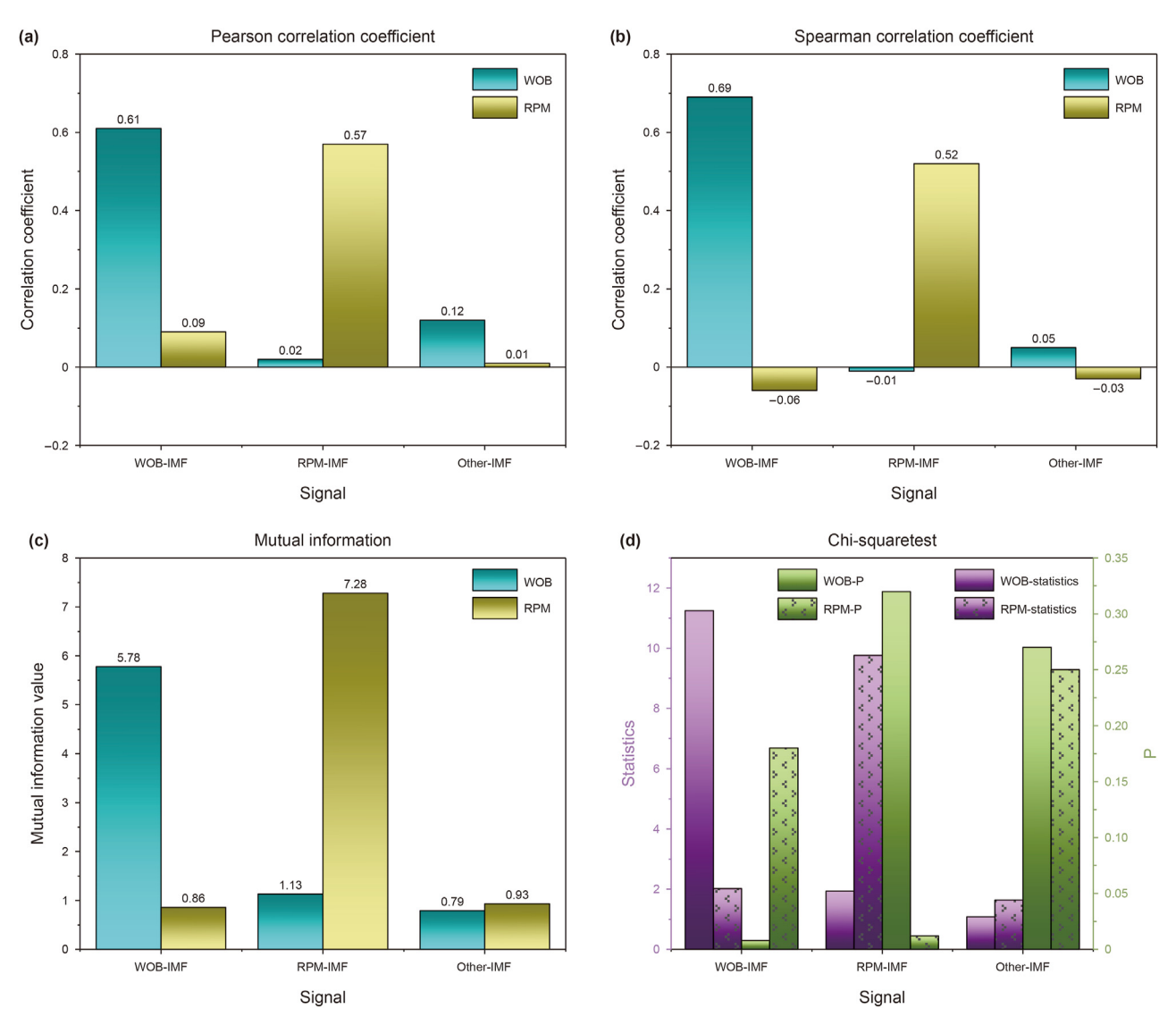


Fig. 10. Verification of signal reconstruction results.

Therefore, in engineering applications, WOB and RPM can be adjusted separately based on the prediction model of WOB-IMF and the prediction model of RPM-IMF to optimize ROP.

The reconstructed signals should have lower signal complexity compared with the original signal. The evaluation of reconstructed signal complexity is similar to the signal complexity evaluation in Section 3.1, and the evaluation of this necessary condition is achieved by the permutation entropy and approximation entropy. By calculating the permutation entropy and approximate entropy of the three reconstructed signals, the calculation results show that the permutation entropy and approximate entropy of the three reconstructed signals are significantly lower compared with the original ROP signal. Moreover, the permutation entropy and approximate entropy of WOB-IMF and RPM-IMF are much lower than the permutation entropy and approximate entropy of Other-IMF (Fig. 11).

By verifying the correspondence between the reconstructed signals and physical parameters, as well as the complexity of the reconstructed signals, it can be concluded that the reconstructed signals have a lower complexity and are easier to predict. The physical meaning of the reconstructed signals is clear, it is easier to control and optimize parameters through models in practical

applications.

## 3.3. Prediction results of different models

In this study, based on the TCN prediction model, the EEMD-BN-TCN prediction model was established by introducing the EEMD signal decomposition and BN causal inference. This section mainly analyzes the differences between the prediction results of EEMD-BN-TCN and those of TCN and EEMD-TCN. Moreover, the prediction results of the EEMD-BN-TCN model were compared and analyzed with the prediction results from five machine learning models: random forest (RF), artificial neural network (ANN), support vector regression (SVR), long short-term memory neural networks (LSTM), and GBDT. The selection of hyperparameters for machine learning models can significantly affect the model's prediction performance. In this study, the hyperparameters for LSTM, GBDT, SVR, ANN, and RF were all obtained using the PSO algorithm. The optimization process of some of the main hyperparameters in the above model is shown in Fig. 12, and the optimization process of other hyperparameters is the same. The specific hyperparameter combinations of these algorithms are shown in Table 3.

In the EEMD-TCN model, the eight sub-signals are first predicted

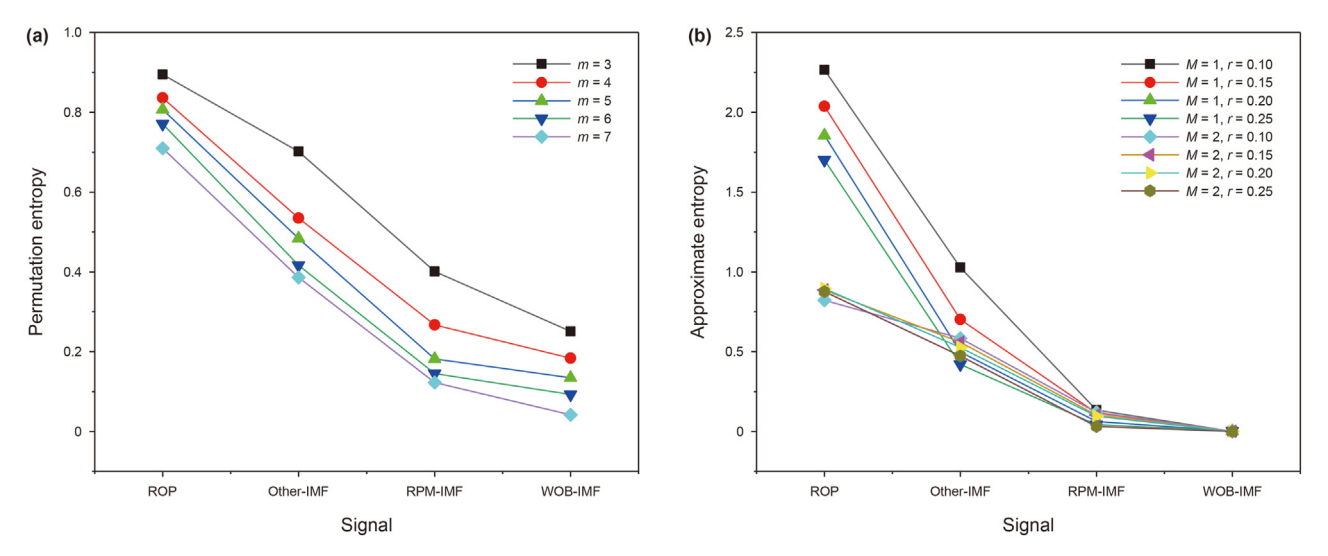


Fig. 11. Reconstructed signal complexity evaluation.

based on the TCN to get the prediction results of each sub-signal. Finally, the prediction results of sub-signals are reconstructed based on the inverse principle of EEMD to get the prediction results of the ROP (Fig. 13). The complexity of the signals will seriously affect the prediction accuracy. The IMF1, IMF2, IMF3, IMF4, IMF5, IMF6, and IMF7 are stationary signals with gradually decreasing complexity (Fig. 7), and overall the MAPE of the prediction results of these seven sub-signals is also gradually decreasing, and the  $R^2$  is gradually increasing (Figs. 13 and 15). The residual signal is a nonstationary monotonous signal, and the MAPE of residual signal is the lowest among the eight sub-signals, and  $R^2$  is the highest (Figs. 13 and 15). This phenomenon is mainly because residual is a simple monotonous decreasing signal, and the complexity of the residual signal is low compared to the other seven sub-signals. The accuracy and error of the final ROP prediction depend on the prediction results of the eight sub-signals, but the prediction error is not a simple superposition of errors of the eight sub-signals. The MAPE of EEMD-TCN is 13.5% and the  $R^2$  of EEMD-TCN is 0.88, while the MAPE of TCN and  $R^2$  of TCN are 18.4% and 0.75, respectively (Fig. 13). It can be seen that signal decomposition by EEMD can effectively improve the prediction accuracy of the TCN model because of the low complexity of the decomposed signal. In addition, the prediction results of EEMD-TCN are jointly determined by the prediction results of eight sub-signals, so even if the prediction accuracy of individual sub-signals is low, it will not have a great impact on the overall prediction results. So the EEMD-TCN model has a stronger robustness compared with TCN.

Although the EEMD-TCN model has better prediction performance than the TCN model, the prediction error of the final ROP is jointly determined by the prediction errors of the eight sub-signals, and each sub-signal contributes to the final prediction error, so the number of sub-signals affects the prediction error to a certain extent. The signal reconstruction is carried out by the BN model, and the eight sub-signals are reconstructed into three sub-signals (WOB-IMF, RPM-IMF, and Other-IMF), which are modeled and predicted individually (Fig. 14). The MAPE of the EEMD-BN-TCN and R<sup>2</sup> of the EEMD-BN-TCN are 9.2% and 0.93, respectively. Compared with EEMD-TCN and TCN, EEMD-BN-TCN had significantly lower MAPE and higher  $R^2$  (Fig. 16(b)). Compared with TCN, the improved prediction accuracy of EEMD-BN-TCN is mainly due to its decomposition of the complex ROP signals into the relatively simple WOB-IMF, RPM-IMF, and Other-IMF. The higher prediction accuracy of EEMD-BN-TCN compared with EEMD-TCN is due to

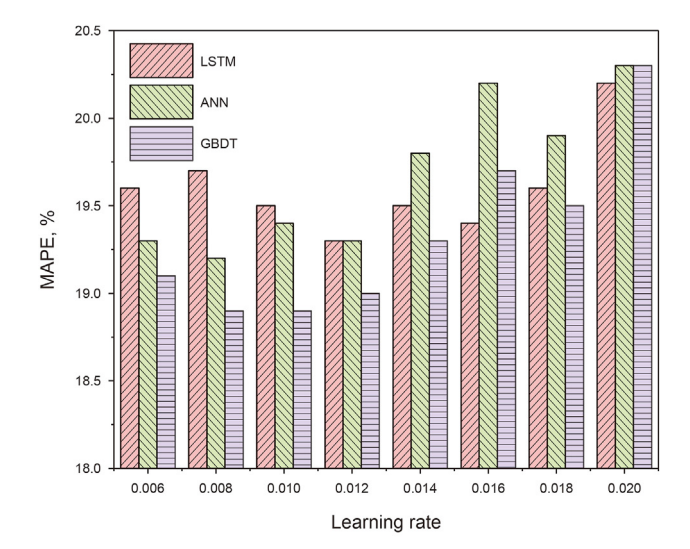
reorganization of the eight signals into three, and the sources of prediction error are changed from eight parts to three parts. The sources of prediction error are reduced, so the prediction accuracy is improved. For the prediction results of EEMD-BN-TCN, WOB-IMF has the highest prediction accuracy among the three sub-signals (Fig. 16(a)), and it can be seen from the image (Fig. 9) that WOB-IMF is an approximately monotonous low-frequency signal, and therefore its prediction difficulty is the lowest. Other-IMF is the one with the highest error among the three sub-signals (Fig. 16(a)). Other-IMF is an approximately stationary high-frequency signal, and the higher frequency of change adds difficulty to the prediction, resulting in a large prediction error for Other-IMF (Fig. 9).

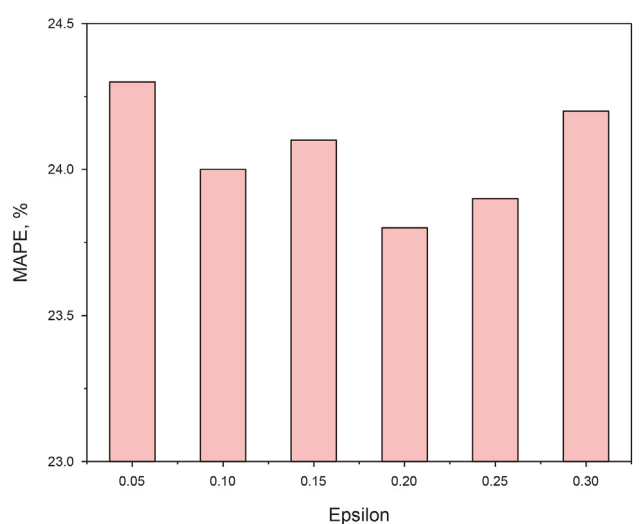
Through the comparative analysis above, it can be concluded that the prediction error of the model gradually decreases during the process of continuous improvement. Moreover, whether the EEMD-BN-TCN model offers advantages over the machine learning models in existing studies is also an important consideration in this research. This study compares the EEMD-BN-TCN model with LSTM, ANN, RF, SVR, and GBDT. The results showed that the error of the TCN model in directly predicting ROP was slightly lower than the five machine learning models mentioned above (Figs. 16(b) and 17). The EEMD-BN-TCN model achieves smaller prediction errors and demonstrates superior predictive performance (Fig. 17). Compared to other models, EEMD-BN-TCN improves prediction accuracy by decomposing complex signals into simpler, more regular signals for analysis and prediction.

# 3.4. The impact of sub-signals on prediction errors

By EEMD, the complex signal is decomposed into several signals with lower complexity, and the prediction difficulty of each subsignal is greatly reduced compared with the original signal, and the prediction accuracy is higher. However, for the final prediction result, each sub-signal will have a prediction error, and these errors will have an impact on the overall errors. Therefore, this section mainly analyzes the relationship between prediction errors of the sub-signals and the final prediction errors and the relationship between prediction errors of the sub-signals and the signal complexity.

To intuitively reflect the relationship between the prediction errors of the sub-signals and the overall prediction errors, Eq. (23) defines the mean absolute error MAE $_j$  of each sub-signal, while the mean absolute error of the final ROP can be expressed as MAE (Eq.





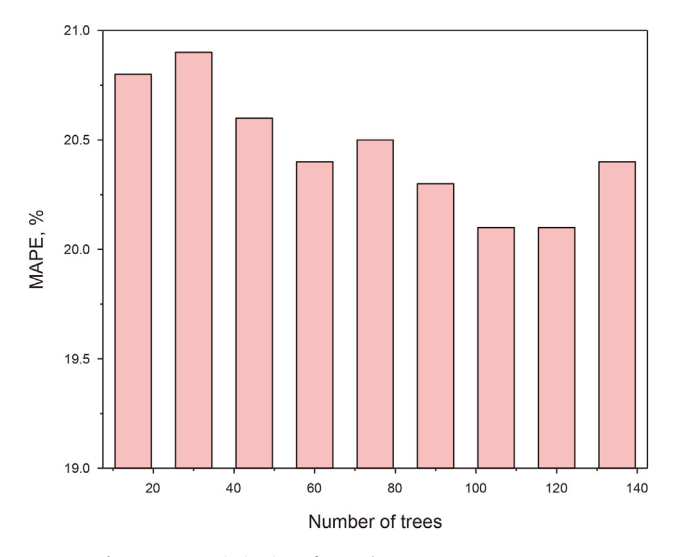


Fig. 12. PSO optimization of some hyperparameter processes.

(25)). Through Eq. (23), the sum of the mean absolute errors of the prediction results of each sub-signal can be known as MAES (Eq. (24)). To clarify the relationship between MAES and MAE, the classical triangular inequality (Eq. (27)) is introduced here, which

still holds when the number of the parameters is increased to any number. Replacing the parameters of Eq. (27) with Eq. (28) can obtain Eq. (29) and Eq. (30), and combining Eq. (24) and Eq. (25) with Eq. (30) can obtain the inequality of Eq. (31). From Eq. (31), it can be seen that the mean absolute error MAE of the final ROP is less than or equal to the sum of the mean absolute error MAES of each sub-signals. The condition that the equal sign of Eq. (31) is established is that the positive and negative signs of each parameter substituted into the triangular inequality are the same, namely, all the prediction results are greater than the original results or are less than the original results.

$$|a+b| \le |a|+|b| \tag{27}$$

$$a = \tilde{y}_{i,1} - y_{i,1}, b = \tilde{y}_{i,2} - y_{i,2}$$
 (28)

$$|a+b+...| = |\tilde{y}_{i,1} - y_{i,1} + \tilde{y}_{i,2} - y_{i,2} + ...| = \left| \sum_{j=1}^{m} \tilde{y}_{i,j} - \sum_{j=1}^{m} y_{i,j} \right|$$

$$\leq \sum_{j=1}^{m} |\tilde{y}_{i,j} - y_{i,j}|$$
(29)

$$\frac{1}{n} \sum_{i=1}^{n} \left| \sum_{j=1}^{m} \tilde{y}_{i,j} - \sum_{j=1}^{m} y_{i,j} \right| \le \frac{1}{n} \sum_{i=1}^{n} \sum_{j=1}^{m} \left| \tilde{y}_{i,j} - y_{i,j} \right|$$
(30)

$$MAE \leq MAES$$
 (31)

$$MAES < MAET$$
 (32)

Eq. (31) quantifies the relationship between the sub-signal prediction errors and the final prediction errors, which also explains the phenomenon that the prediction errors of the EEMD-TCN are larger than the EEMD-BN-TCN prediction error. Because the sum of the final sub-signal errors (MAES) is larger when there are more sub-signals, the upper limit of the final prediction error increases. Eq. (31) can also be used to initially analyze the reasonableness of the decomposed signals. If the mean absolute error of the TCN direct prediction of ROP is remembered as MAET, MAES  $\leq$  MAET (Eq. (32)) is a necessary condition for the reasonableness of the signal decomposition. When MAES < MAET, it also means MAE < MAET, namely, the mean absolute error of the EEMD-TCN will not exceed the mean absolute error of the TCN direct prediction. All in all, Eq. (32) determines the upper limit of the final error, so it can serve as a necessary condition for reasonable signal decomposition.

The MAES of both EEMD-TCN and EEMD-BN-TCN is smaller than the MAET of TCN, which satisfies Eq. (32), namely, a necessary condition for decomposition is met (Fig. 18). In the prediction results of EEMD-TCN, the final mean absolute error is smaller than the sum of the mean absolute errors of the eight sub-signals, and the above results satisfy Eq. (32) (Fig. 18). Similarly, the prediction results of EEMD-BN-TCN also satisfy Eq. (32). The mean absolute errors of different sub-signals are not comparable due to the large difference in their value ranges, but the threshold widths of the seven sub-signals (from IMF1 to IMF7) are similar, while the mean absolute errors are reduced in turn, because the complexity of these seven sub-signals is reduced in turn (Fig. 18).

According to the prediction results in Section 3.3, it can be intuitively perceived that the signal complexity has an important influence on the prediction accuracy (Figs. 7 and 15, Figs. 11 and 16). In this study, the signal complexity is mainly quantitatively

**Table 3**Determination of machine learning algorithm hyperparameters.

Method	Range of hyperparameter	Hyperparameter
LSTM	Learning rate = [0.001, 0.3], Hidden units = [16, 1024]	Number of layers = 3, Learning rate = 0.016, Hidden units=(64, 128, 256)
GBDT	Number of trees = $[25, 500]$ , Learning rate = $[0.001, 0.3]$ , Max depth = $[1,20]$	Number of trees $= 135$ , Learning rate $= 0.01$ , Max depth $= 8$ , Subsample $= 0.9$
SVR	Epsilon = $[0.01, 0.5]$ , Regularization parameter = $[0.01, 100]$	Kernel = 'rbf', Epsilon = 0.2, Regularization parameter = 10
ANN	Learning rate = $[0.001, 0.3]$ , Hidden units = $[16, 1024]$	Number of layers = 4, Learning rate = 0.008, Hidden units=(64, 128, 256, 64)
RF	Number of trees $=$ [10, 500], Max depth $=$ [1, 50], Min samples split $=$ [1, 20]	Number of trees $= 105$ , Max depth $= 8$ , Min samples split $= 6$

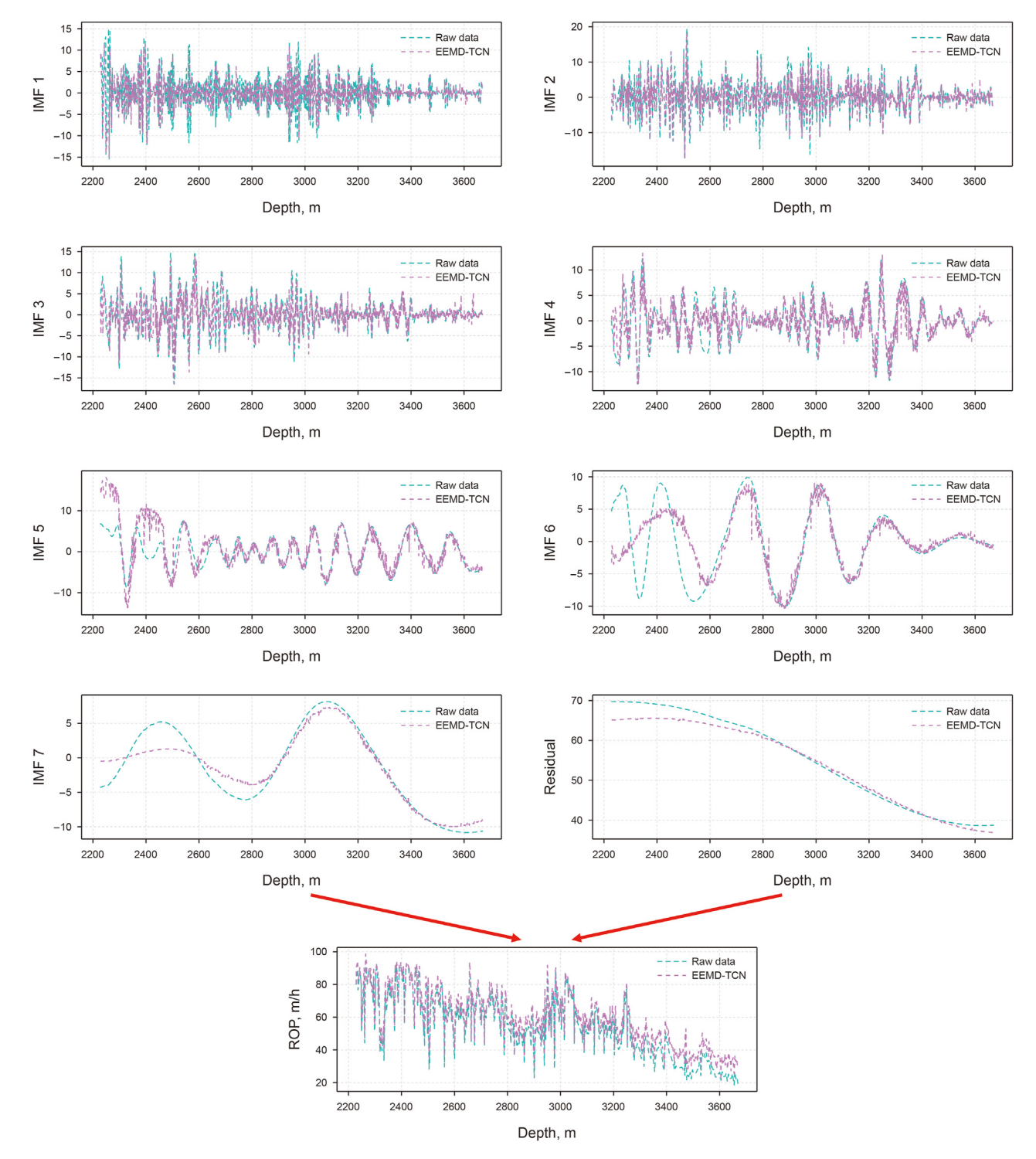


Fig. 13. Prediction results of the EEMD-TCN.

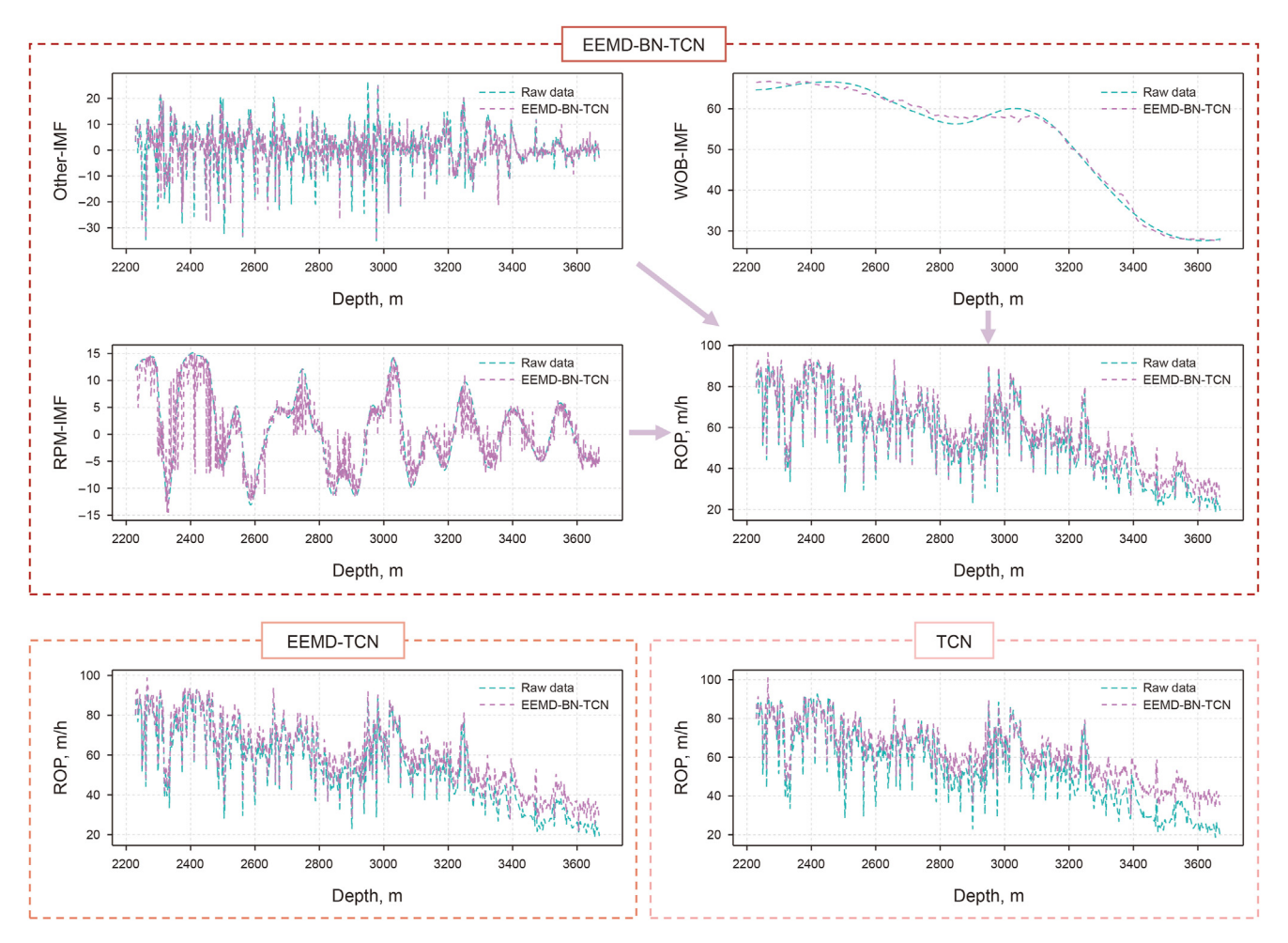


Fig. 14. Comparison of prediction results of multiple models.

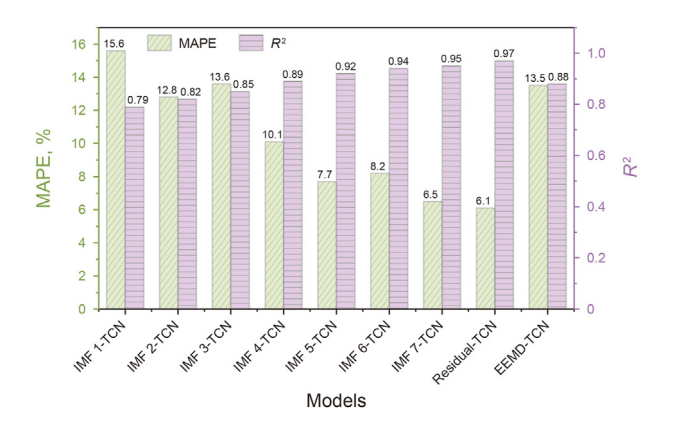


Fig. 15. Prediction errors of the EEMD-TCN.

described by the permutation entropy and the approximate entropy, while the prediction accuracy is mainly quantitatively described by the MAPE and the  $\mathbb{R}^2$ . Therefore, we focus on analyzing the relationship between the permutation entropy, approximation entropy and errors (MAPE and  $\mathbb{R}^2$ ) for each sub-signal. The main parameter of permutation entropy (m) is taken as 5, while the main parameters of approximation entropy (M and P) are taken as 2 and 0.1, respectively.

In general, there is a positive correlation between MAPE and

signal complexity (permutation entropy and approximation entropy), indicating that higher permutation entropy and approximation entropy values correspond to larger MAPE values (Fig. 19). The negative correlation is shown between the  $R^2$  and the signal complexity (arrangement entropy and approximation entropy), indicating that higher permutation entropy and approximation entropy values correspond to lower  $R^2$  values (Fig. 19). Among the 11 sub-signals of EEMD-TCN and EEMD-BN-TCN, the MAPE of residual and WOB-IMF is lower than the other sub-signals, and the  $R^2$  of residual and WOB-IMF is higher than the other sub-signals (Fig. 19). The frequency of residual and WOB-IMF is the lowest of these sub-signals, and residual is a monotonous signal, while WOB-IMF is also approximately monotonous. This shows that monotonic low-frequency signals have lower signal complexity, and the prediction accuracy is high because of their lower complexity.

The EEMD-BN-TCN model ensures low prediction error, which is directly related to the complexity of the signals. The final prediction result of the EEMD-BN-TCN model is obtained by separately predicting the WOB-IMF, RPM-IMF, and Other-IMF components. Since the signal complexity of WOB-IMF and RPM-IMF is relatively low, their prediction errors are also smaller (Fig. 19). Although the signal complexity of Other-IMF is higher, its signal amplitude is very small (Fig. 9), meaning the final prediction result is primarily determined by WOB-IMF and RPM-IMF. Even if the prediction error of Other-IMF is relatively large, its impact on the final ROP prediction result is minimal. This is a key factor contributing to the high accuracy of the EEMD-BN-TCN model.

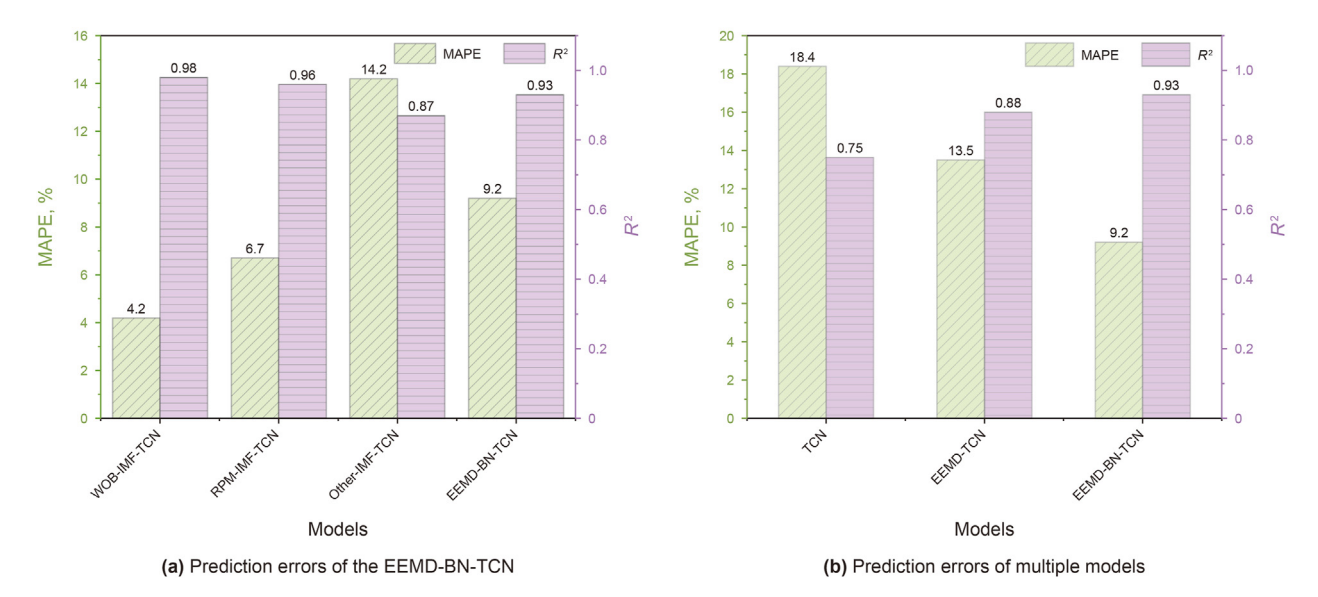


Fig. 16. EEMD-BN-TCN and other model prediction error.

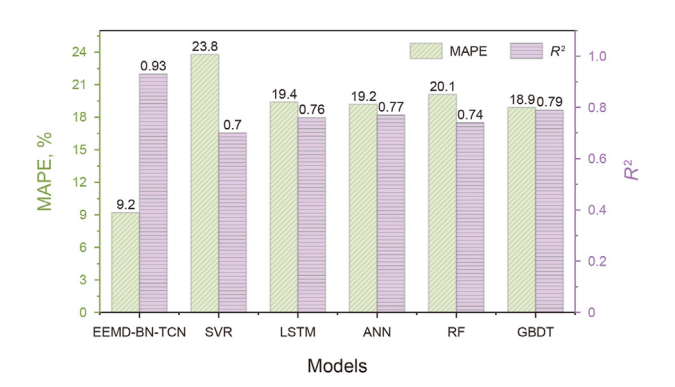


Fig. 17. Comparison of prediction errors between the EEMD-BN-TCNN and other models.

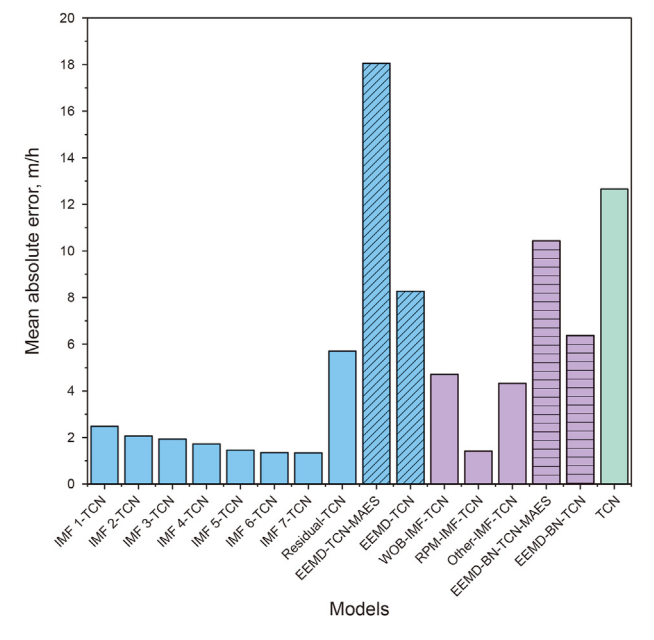


Fig. 18. Absolute errors of prediction results.

#### 4. Discussion

## 4.1. The influence of signal attributes on prediction results

The sub-signals after EEMD decomposition show different characteristics, and the frequency and amplitude of sub-signals are different (Figs. 6 and 9). The difficulty of signal prediction varies with different time-frequency characteristics, and the influence of sub-signals with different time-frequency characteristics on the final prediction results also varies. In this section, the time-frequency analysis of the sub-signals is first performed by wavelet transform, and the importance of different sub-signals for final ROP prediction is analyzed by the signal importance defined in this section.

Wavelet transform can realize the time-frequency transformation of the signals, to obtain the time-frequency characteristics of the signals. The time-frequency analysis is carried out on the signals through the wavelet transform, in which the maximum frequencies of IMF1, IMF2, IMF3, and IMF4 are all over 100 Hz, while the maximum frequencies of the residual signal, IMF5, IMF6, and IMF7 are all below 100 Hz (Fig. 20). For the time-frequency variation of each signal, the signal intensity (amplitude of the z-axis) in its low-frequency region is greater than that in the high-frequency region, namely, the main information is stored by the region with a relatively low frequency. Among the eight sub-signals of EEMD, the maximum intensity of the residual signal is the highest, followed by the maximum signal intensity of IMF6. For the EEMD-TCN, the prediction results of residual and IMF6 have the greatest impact on the final prediction results (Fig. 20). For the reconstructed signals by the EEMD-BN, the frequency of the Other-IMF is higher than that of the WOB-IMF and RPM-IMF, but its signal strength is overall lower than that of the WOB-IMF and RPM-IMF (Fig. 21). The signal strength of WOB-IMF is the largest, which shows the final prediction results are mainly determined by the prediction result of WOB-IMF, followed by the prediction result of RPM-IMF, while Other-IMF has the least influence on the final prediction result.

Time-frequency analysis based on wavelet transform can intuitively determine the impact of different sub-signals on the final prediction results, but it cannot quantitatively analyze the above relationship. To quantify the degree of importance of each subsignal for the final results, the signal importance (SI) is defined in

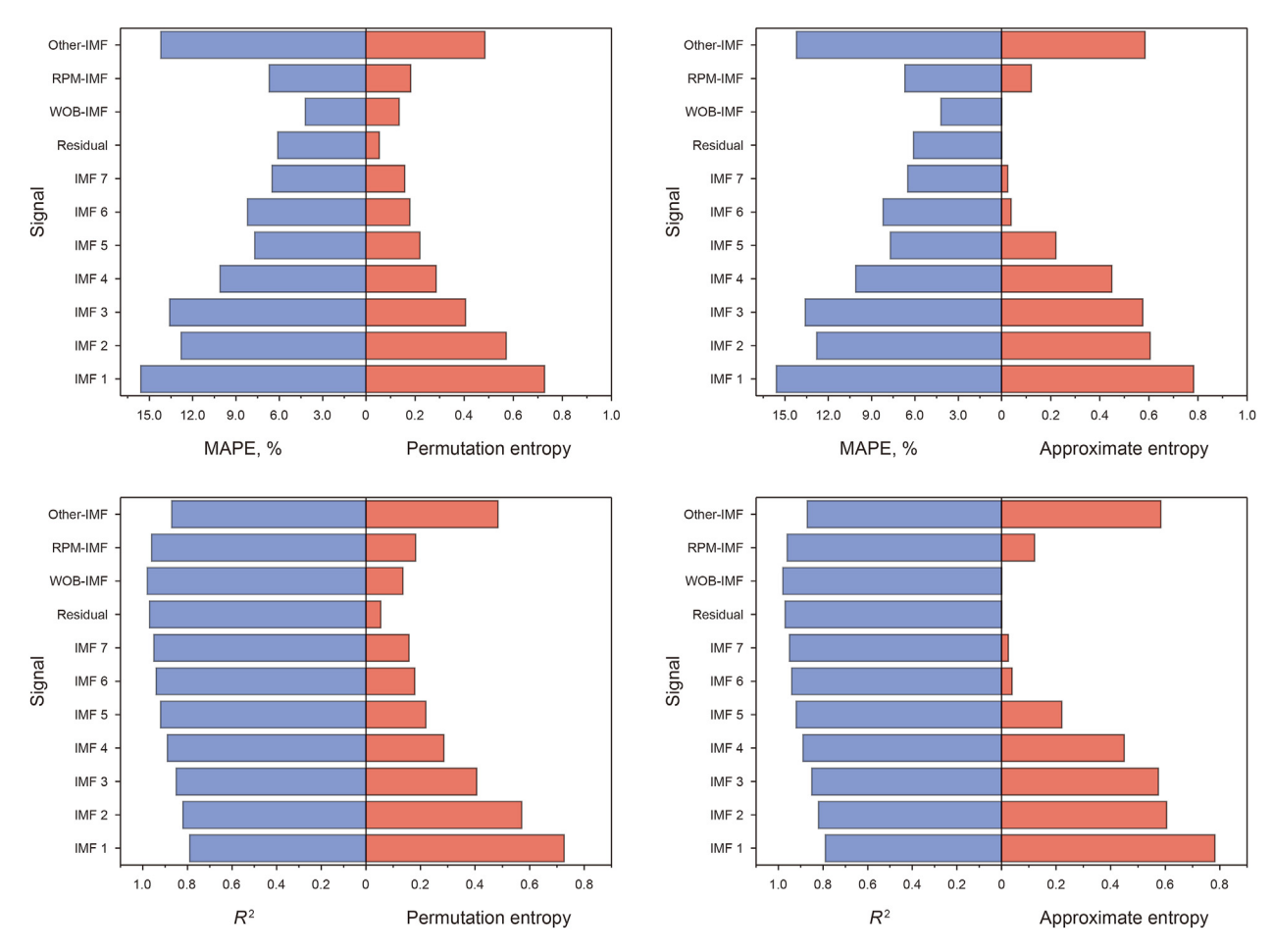


Fig. 19. Signal complexity and prediction accuracy.

this study. Taking the prediction results of EEMD-TCN as an example, one sub-signal is reduced each time, and the prediction results of the remaining seven sub-signals are reconstructed into the final prediction results of the ROP signal. At this point, the absolute relative error of the ROP prediction result can be expressed as Eq. (33). If the absolute relative error significantly increases after reducing a certain sub-signal, it can be considered that the sub-signal has a significant impact on the final prediction result. The signal importance of sub-signals based on absolute relative error is defined by Eq. (34), and the average signal importance of sub-signals is defined by Eq. (35).

$$ARE_{k,i} = \frac{\left| \sum_{j=1}^{k-1} \tilde{y}_{j,i} + \sum_{j=k+1}^{m} \tilde{y}_{j,i} - y_i \right|}{y_i} \times 100\%$$
 (33)

$$SI_{k,i} = \frac{ARE_{k,i}}{\sum\limits_{k=1}^{m} ARE_{k,i}}$$
(34)

$$MSI_{k} = \frac{\sum_{i=1}^{n} SI_{k,i}}{\sum_{k=1}^{m} \sum_{i=1}^{n} SI_{k,i}}$$
(35)

where  $ARE_{k,i}$  is the absolute relative error of the prediction result after removing the prediction result of the sub-signal k,  $\tilde{y}_{j,i}$  is the prediction result of the sub-signal j, m is the total number of subsignals (for EEMD-TCN and EEMD-BN-TCN, it is 8 and 3, respectively),  $y_i$  is the real result,  $SI_{k,i}$  is the signal importance of the subsignal k, and  $MSI_k$  is the mean signal importance of the sub-signal k.

For the eight sub-signals after the EEMD-TCN decomposition, the residual signal has the greatest impact on the final prediction results, followed by IMF7, IMF6, and IMF5 (Fig. 24(a)). This is consistent with the results of the wavelet transform time-frequency analysis, indicating that the final prediction results are mainly determined by four signals with lower frequencies (Figs. 20 and 24(a)). For the data at different depths, the importance is also different. IMF1, IMF2, IMF3, IMF4, and IMF6 have very low importance for the data at deeper depths (from 3300 to 3669 m), while residual and IMF7 have high importance for the data at the above depths, so it can be seen that the prediction results of the data at the above depths are mainly determined by IMF7 and residual (Fig. 22). IMF5 has the highest importance for the data from 2154 to 2493 m, and IMF5 mainly affects the prediction accuracy of the data at the above depths, while it has less effect on the other data.

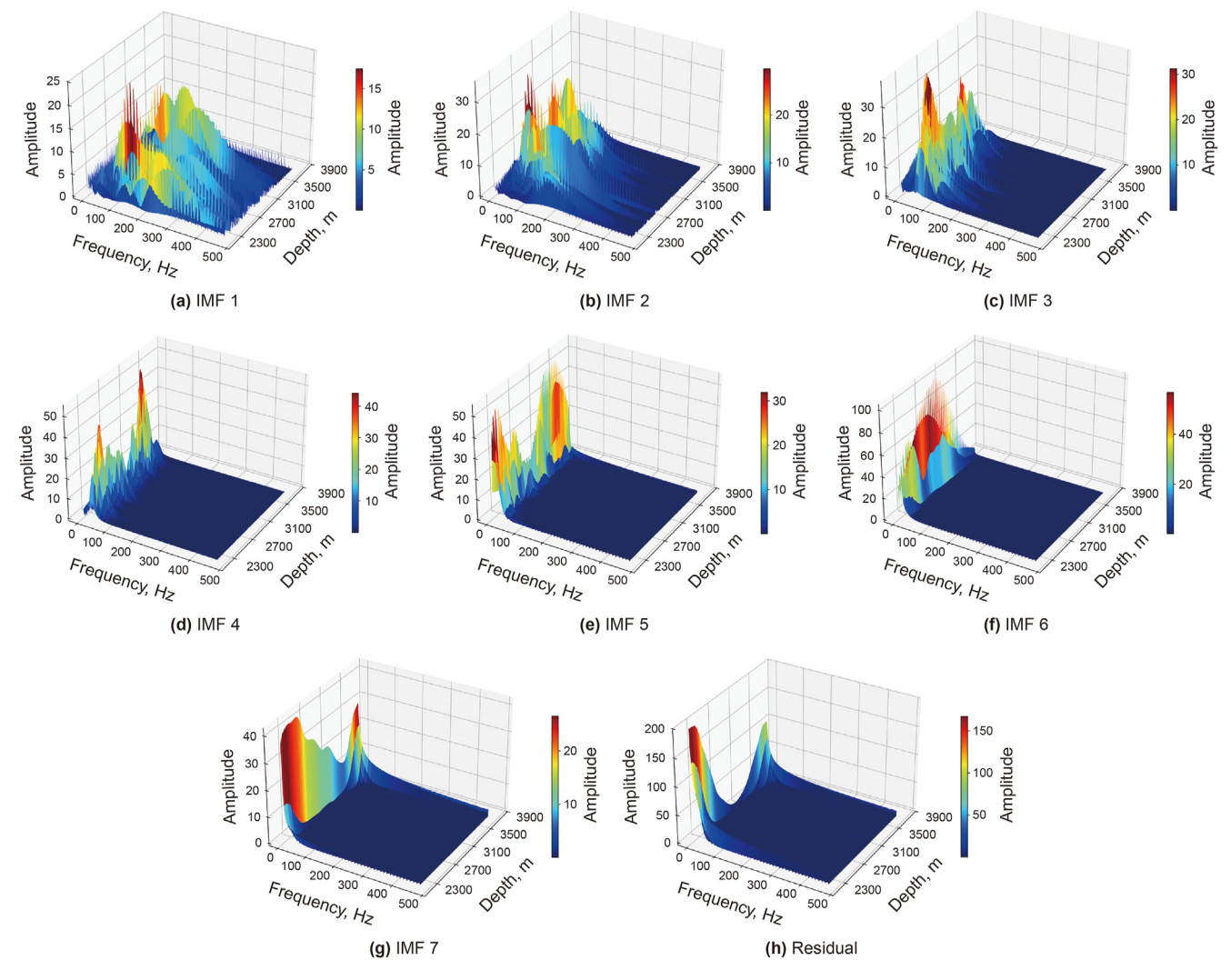


Fig. 20. EEMD decomposition signal time-frequency analysis.

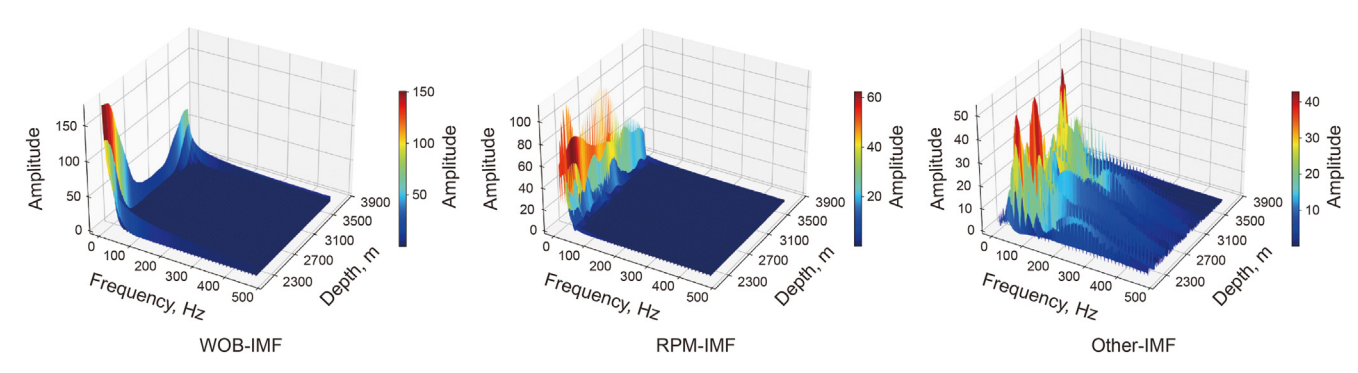


Fig. 21. Time-frequency analysis of EEMD-BN reconstructed signals.

Therefore, for the EEMD-TCN model, the prediction accuracy of the residual should be considered first. For IMF5, the prediction accuracy of the data with shallow depths is mainly considered. IMF7 mainly affects the prediction accuracy of the data from 3300 to 3669 m (deeper depth), IMF6 mainly affects the prediction accuracy of the data from 3300 to 3669 m (deeper depth), while IMF4 mainly affects the prediction accuracy of the data from 3200 to 3300 m (moderate depth).

For the EEMD-BN-TCN, the WOB-IMF has the highest importance with an average signal importance of 82.6%, while the RPM-IMF and Other-IMF have an average signal importance of 9.3% and 8.1%, respectively (Fig. 24(b)). The WOB-IMF is more important for data at all depths, and the RPM-IMF is more important for data from 2154 to 2493 m, while Other-IMF is more important for data from 2564 to 3276 m (Fig. 23). Therefore, for the EEMD-BN-TCN, the prediction accuracy of WOB-IMF should be ensured firstly. For

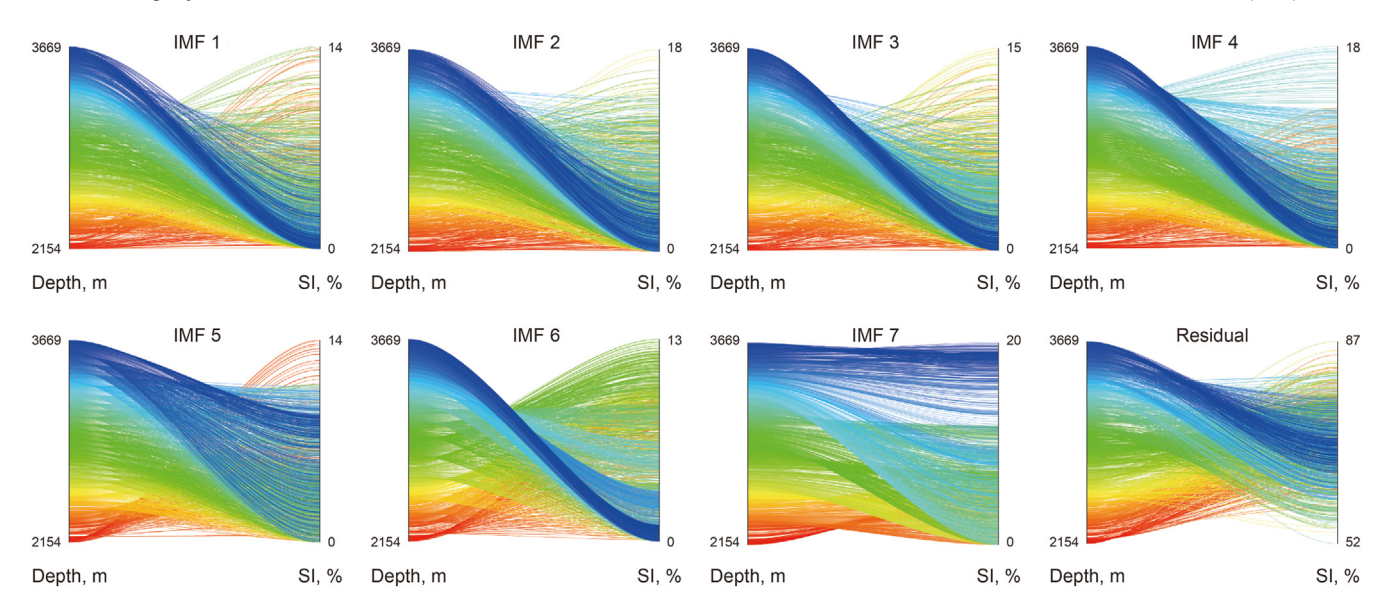


Fig. 22. Parallel plot of EEMD-TCN signal importance analysis.

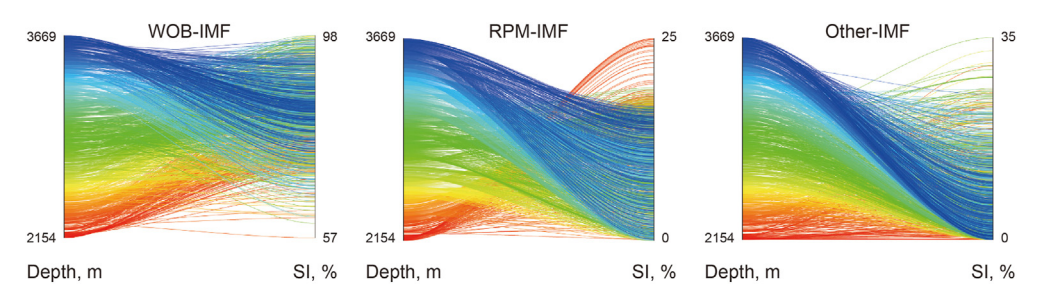


Fig. 23. Parallel plot of EEMD-BN-TCN signal importance analysis.

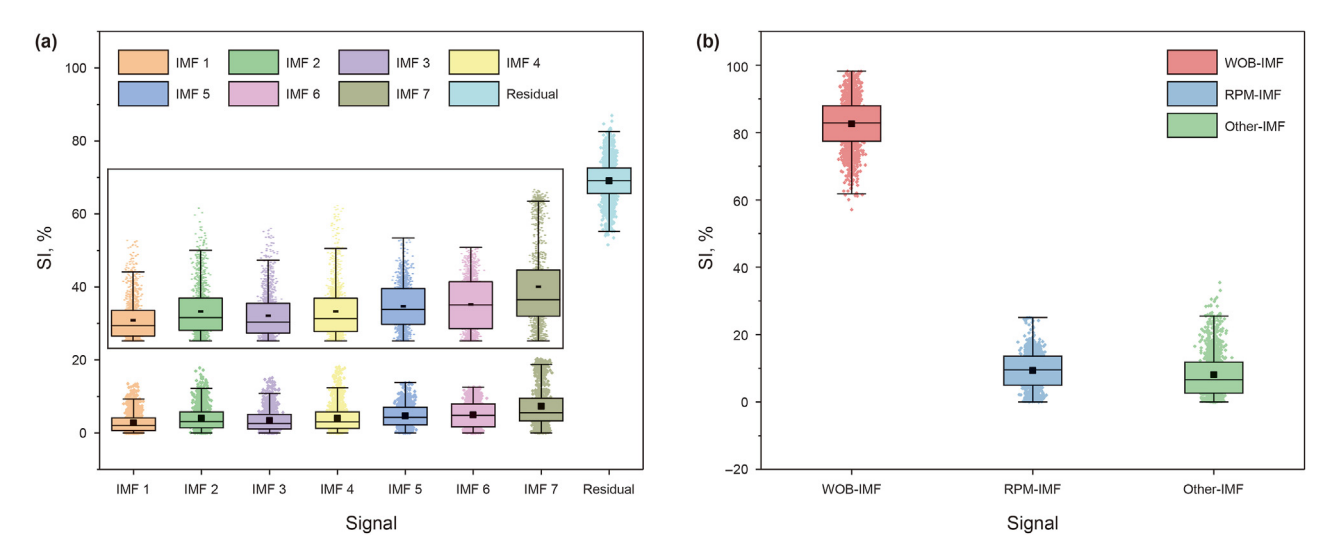
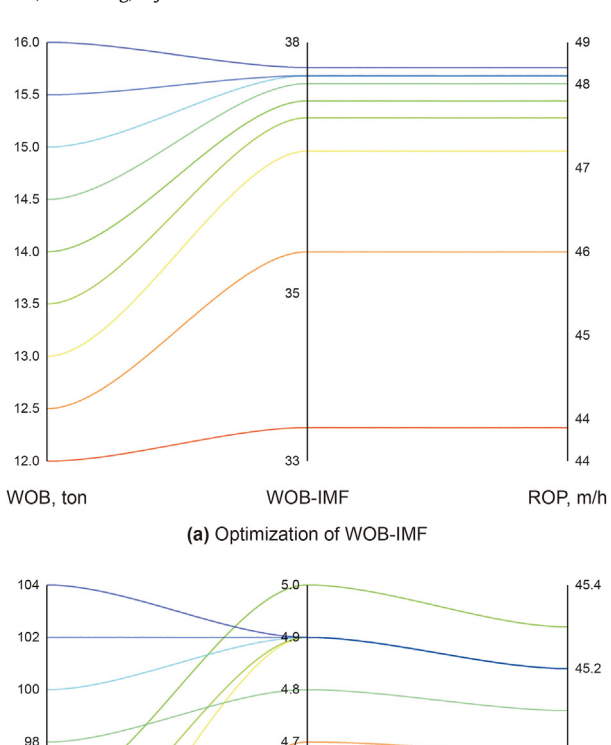


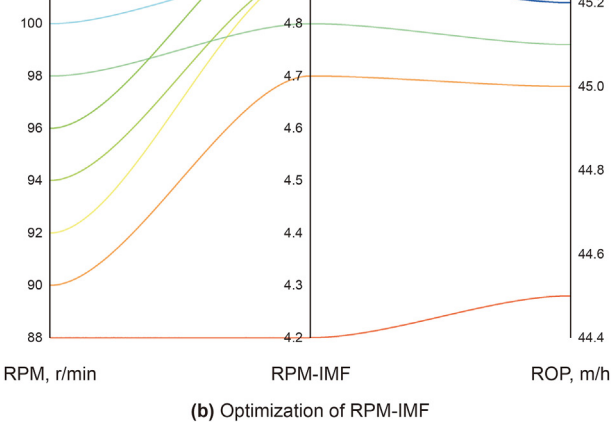
Fig. 24. Analysis of the importance of different signals.

RPM-IMF, the prediction accuracy of data with shallower well depths should be given special consideration, while Other-IMF should especially consider the prediction accuracy of data with centered well depths.

In conclusion, the prediction results of different sub-signals have different degrees of influence on the prediction results of

the final ROP. Overall, the low-frequency signals have a greater influence on the final prediction results, while the same signal has a different degree of influence on the final prediction results of the data at different depths.





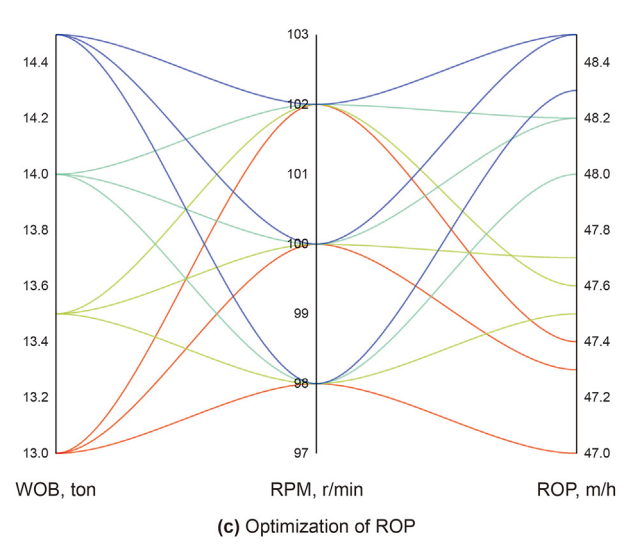


Fig. 25. Regulation of WOB and RPM to optimize ROP at well depth 3401 m.

## 4.2. The significance of the model in regulating physical parameters

WOB and RPM are two parameters that are highly correlated with ROP, and they are also two parameters that can be artificially

regulated during the construction process. So WOB and RPM can be regulated according to the EEMD-BN-TCN model, so that ROP can be improved during drilling, and the drilling cost can be reduced. For the EEMD-BN-TCN model, since the WOB is only related to the WOB-IMF, only the change of WOB-IMF needs to be paid attention to when regulating the WOB. Similarly, only the change of RPM-IMF needs to be paid attention to when regulating the RPM. The final optimization result of ROP is determined by the optimization results of WOB-IMF and RPM-IMF together. The Other-IMF is not optimized, but the final optimized ROP is composed of the unoptimized Other-IMF together, the optimized WOB-IMF, and the optimized RPM-IMF.

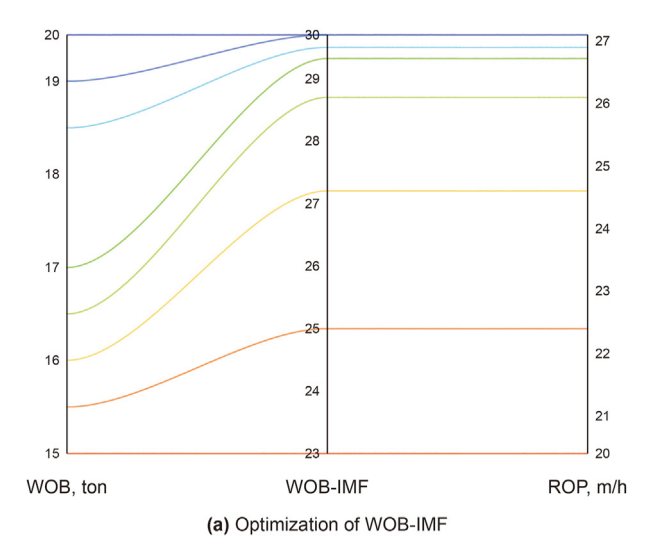
Taking the data from well depths of 3400 and 3600 m as examples, based on the EEMD-BN-TCN model, WOB-IMF and RPM-IMF were optimized by regulating WOB and RPM to achieve ROP optimization. WOB-IMF reaches 37.6 when WOB is 15.5 ton, and then the ROP is increased to 48.4 m/h (Fig. 25(a)). When RPM is regulated at 96 r/min, RPM-IMF reaches 5.0, and then the ROP is increased to 45.3 m/h (Fig. 25(b)). For the above data, WOB regulation has a greater impact on ROP compared to RPM regulation. When WOB and RPM are regulated simultaneously, the ROP increases to 48.5 m/h when WOB and RPM are 14.5 ton and 102 r/min respectively, while the original ROP here is 34.8 m/h (Fig. 25(c)). For the data at the depth of 3660 m, when WOB and RPM are regulated separately, the ROP can be increased to 27.1 and 26.8 m/h, respectively, and the final ROP can be increased to 28.4 m/h when WOB and RPM are regulated at the same time, while the original ROP here is 23.1 m/h. This shows that regulating WOB and RPM with the help of the EEMD-BN-TCN model can effectively improve ROP, thus saving drilling time and drilling costs. In the process of regulation, the increase of ROP is more obvious by regulating WOB, therefore, in the subsequent regulation, the main focus is to optimize WOB-IMF by regulating WOB to improve ROP, while the RPM regulation is auxiliary (see Fig. 26).

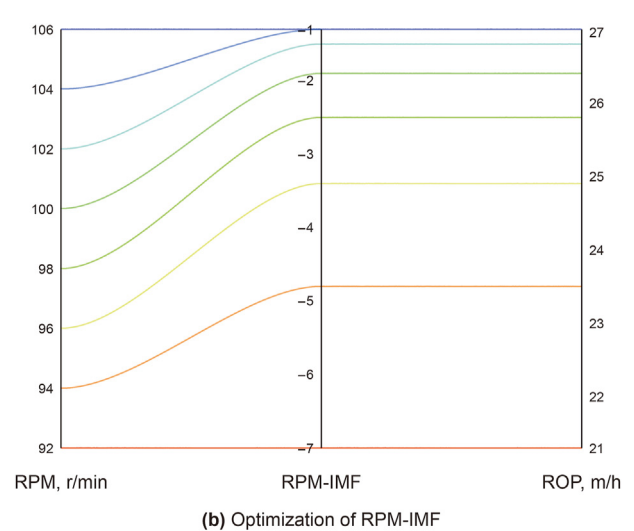
The previous analysis focused on optimizing ROP by regulating WOB and RPM for individual data. However, for drilling wells, increasing ROP at a certain depth does not change the overall drilling time significantly, so here a piece of continuous data is selected to analyze the change of ROP by regulating WOB and RPM. In the ten sets of data in the range of 3401-3410 m, the range of WOB-IMF predicted and RPM-IMF predicted are 32-35 and 3-5, respectively, and the corresponding range ROP predicted is from 38 to 46 m/h. After optimization, the range of WOB-IMF, RPM-IMF, and ROP is 36–38, 4–5, and 42–49 m/h, respectively (Fig. 27). Overall, for the ten sets of data in the range of 3401-3410 m, WOB-IMF and RPM-IMF can be effectively improved by regulating WOB and RPM, respectively, and finally ROP is also significantly optimized. For the well depth from 3651 to 3660 m, the ROP is generally lower, so we want to improve the ROP by regulating WOB and RPM. Regulating WOB improves the WOB-IMF (Fig. 28(a)), and the RPM-IMF improves less after regulating RPM (Fig. 28(b)), which shows that the effect of WOB on the ROP is greater than the effect of RPM on the ROP. For the above data, the RPM is mainly distributed in 87–102 r/ min, while the WOB is mainly distributed in 5.7-9.2 ton. The RPM approaches the optimal RPM, while the WOB still has a certain range from the optimal WOB, so the effect of regulating the WOB on the final ROP is more obvious.

## 5. Conclusion and limitations

#### 5.1. Conclusion

In this study, the TCN prediction model is improved based on EEMD signal decomposition and BN causal inference, and the EEMD-BN-TCN prediction model adapted to parameters regulation





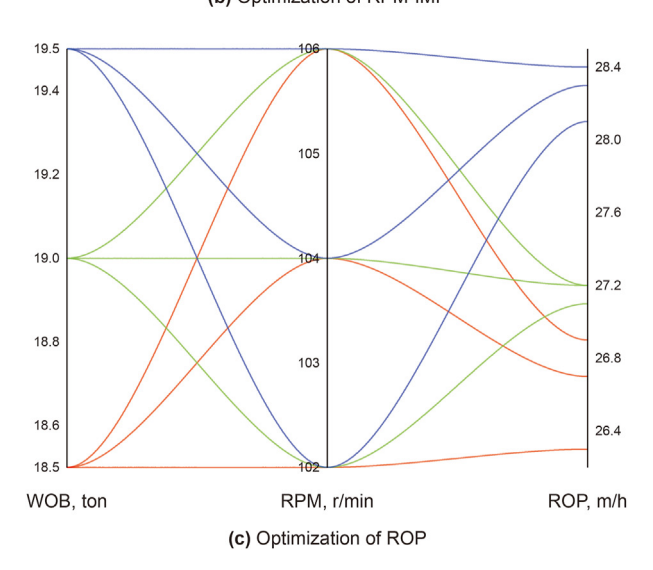


Fig. 26. Regulation of WOB and RPM to optimize ROP at well depth 3660 m.

for engineering applications is proposed. The EEMD-BN-TCN model has three main characteristics compared with the conventional prediction model. Firstly, the model decomposes the complex signals into signals with lower complexity and obvious regularity, and

an evaluation method for signal complexity is proposed. Secondly, the model analyzes the correspondence between the sub-signals and some important physical parameters through causal inference and initially reconstructs the sub-signals according to the analysis results. Thirdly, the model includes several sub-models, which have good correspondence with the actual physical parameters. In practical engineering applications, WOB and RPM can be adjusted independently. When WOB is adjusted, only the WOB-IMF changes (The same applies to RPM). Therefore, it is possible to optimize ROP by independently adjusting WOB and RPM without considering parameter coupling. This approach can effectively shorten the drilling cycle and reduce drilling costs. The following conclusions are drawn from the study.

- (1) EEMD decomposition can reduce the complexity of the original signal, and the decomposed signal often possesses stationarity, periodicity, or monotonicity, which makes it easier for the TCN model to learn the intrinsic laws of the signal and improve the prediction accuracy. For each subsignal, the lower its complexity the lower the prediction error.
- (2) BN causal inference combines the signals related to WOB and RPM to obtain WOB-IMF, RPM-IMF, and the rest of the signals are combined as Other-IMF, which reconstructs the eight sub-signals originally obtained from the decomposition into three sub-signals. Compared with EEMD-TCN, EEMD-BN-TCN reduces the sources of error of the final ROP prediction results from eight to three ways, which further improves the prediction accuracy.
- (3) For the EEMD-TCN model, the most important sub-signal for the final ROP prediction is the residual signal. For the EEMD-BN-TCN model, the sub-signal with the greatest influence on the final prediction is WOB-IMF. In addition, the same subsignal has different importance for data at different depths. According to this rule, corresponding adjustments can be made to different models of sub-signals at different depths to improve prediction accuracy.
- (4) Based on the EEMD-BN-TCN model, the regulation of key physical parameters WOB and RPM can effectively improve the WOB-IMF and RPM-IMF, and thus improve the ROP. The above two sets of parameters are regulated independently, which makes it more convenient for industrial applications, and the regulation of WOB has a greater impact on the improvement of the ROP in general.

# 5.2. Limitations and future work

This study proposes the EEMD-BN-TCN method, which separates the signals related to WOB and RPM from the original ROP signal by signal decomposition and reconstruction. By adjusting WOB and RPM, the WOB-IMF and RPM-IMF are optimized, thereby improving the ROP. This method has high practical value, but due to some objective factors such as research conditions, data collection, and computational power, this study also has certain limitations.

To ensure the model's real-time prediction performance while drilling, the consideration of geological parameters was somewhat limited in this study. Additionally, in the process of optimizing ROP by adjusting physical parameters, this study only considered adjusting WOB and RPM for the sake of practical engineering applications. However, other engineering parameters, such as drilling fluid density, can also be adjusted. The control of drilling fluid density, though, may lead to wellbore stability issues, which is why it was not considered in this study. Furthermore, the EEMD signal decomposition requires the introduction of white noise. Although

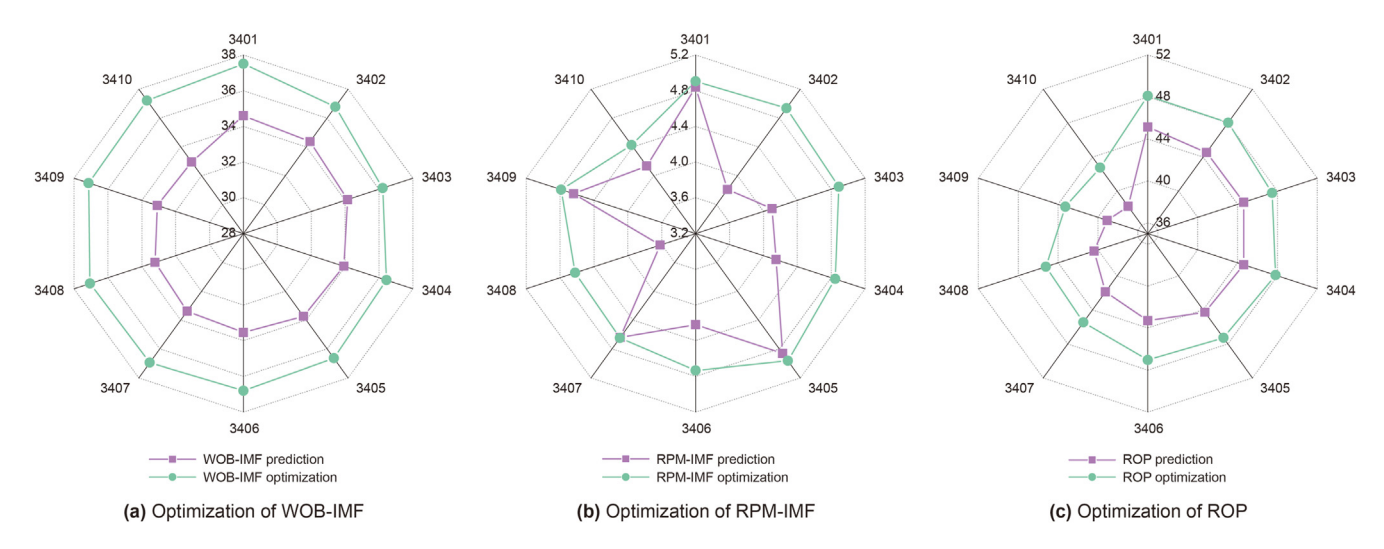


Fig. 27. The data of 3401-3410 m by regulating WOB and RPM to optimize ROP.

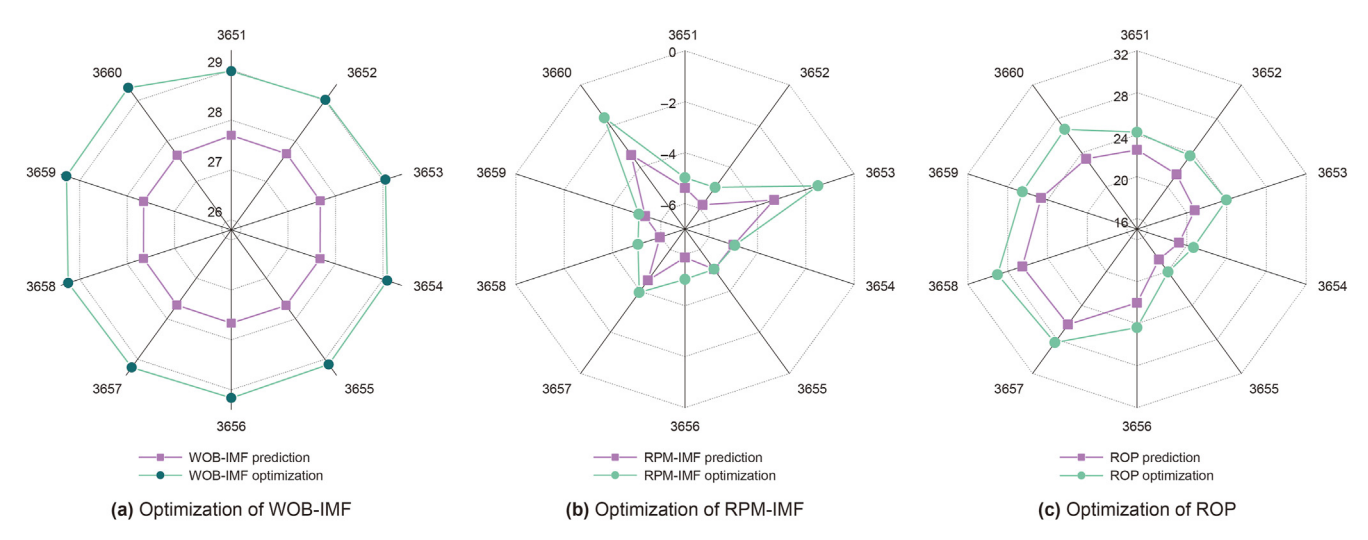


Fig. 28. The data of 3651–3660 m by regulating WOB and RPM to optimize ROP.

the amplitude of the white noise is small and its effect on the results is negligible, it is still an important factor influencing the prediction outcome. This study assumes that the impact of white noise on the results can be ignored. Moreover, the decomposition and prediction process requires significant computational time, which affects the real-time performance of the model. Finally, this study mainly focuses on ROP prediction for vertical wells. However, for inclined wells, horizontal wells, and other types, ROP prediction is more complex. The proposed method can serve as a reference, but it cannot be directly applied. Even for vertical wells, the model needs to be appropriately adjusted for different strata.

In future work, We will consider incorporating some while drilling logging data to improve the accuracy of the prediction results, and also adjust the drilling fluid parameters in combination with wellbore stability. During the decomposition process, we will consider incorporating physical factors into the signal decomposition process to ensure that the decomposed signals align more closely with the variation patterns of specific physical parameters, facilitating parameter control. This can also reduce the number of sub-signals obtained from the signal decomposition, thereby improving computational efficiency to some extent.

## **CRediT authorship contribution statement**

**Yong-Dong Fan:** Writing — original draft, Methodology, Investigation, Data curation. **Hui-Wen Pang:** Writing — review & editing, Methodology, Investigation. **Yan Jin:** Writing — review & editing, Supervision, Resources, Methodology. **Han Meng:** Writing — original draft, Visualization, Validation. **Yun-Hu Lu:** Visualization, Supervision.

# Data availability

Data will be made available on request.

## **Declaration of competing interest**

The authors declare that they have no known competing financial interests or personal relationships that could have appeared to influence the work reported in this paper.

## Acknowledgment

The authors would like to acknowledge gratefully the financial support by the National Natural Science Foundation of China (Grant No. U24B2029), the Key Projects of the National Natural Science Foundation of China (Grant No. 52334001), the Strategic Cooperation Technology Projects of CNPC and CUPB (Grand No. ZLZX2020-02), the China University of Petroleum, Beijing (Grand No. ZX20230042).

#### References

- Ahmad, A.A., Ahmed, A.M., Elkatatny, S., et al., 2022a. Artificial neural networksbased correlation for evaluating the rate of penetration in a vertical carbonate formation for an entire oil field. J. Petrol. Sci. Eng. 208, 109693. https:// doi.org/10.1016/j.petrol.2021.109693.
- Ahmad, A.A., Ahmed, A.M., Elkatatny, S., et al., 2022b. A novel artificial neural network-based correlation for evaluating the rate of penetration in a natural gas bearing sandstone formation: a case study in a middle east oil field. J. Sens., 9444076 https://doi.org/10.1155/2022/9444076.
- Ahmad, A.A., Salaheldin, E., Ahmed, A.M., et al., 2020. Prediction of the rate of penetration while drilling horizontal carbonate reservoirs using the selfadaptive artificial neural networks technique. Sustainability 12 (4), 1376. https://doi.org/10.3390/su12041376.
- Ahmed, A., Salaheldin, E., Hany, G., 2022. Rate of penetration prediction while drilling vertical complex lithology using an ensemble learning model. J. Petrol. Sci. Eng. 208, 109335. https://doi.org/10.1016/j.petrol.2021.109335.
- Bai, S., Kolter, J.Z., Koltun, V., 2018. An empirical evaluation of generic convolutional and recurrent networks for sequence modeling. ArXiv 1803, 01271. https://doi. org/10.48550/arXiv.1803.01271.
- Bingham, M.G., 1965. A New Approach to Interpreting- Rock Drillability. Petroleum Pub. Co, Oklahoma, USA.
- Bourgoyne, A.T., Young, F.S., 1974. A multiple regression approach to optimal drilling and abnormal pressure detection. Soc. Petrol. Eng. J. 14 (4), 371–384. https:// doi.org/10.2118/4238-PA.
- Brenjkar, E., Delijani, E.B., 2022. Computational prediction of the drilling rate of penetration (ROP): a comparison of various machine learning approaches and traditional models. J. Petrol. Sci. Eng. 210, 110033. https://doi.org/10.1016/ j.petrol.2021.110033.
- Chen, P., Zhang, Z., Huang, Y., et al., 2022. Risk assessment of marine accidents with Fuzzy Bayesian Networks and causal analysis. Ocean Coast Manag. 228, 106323. https://doi.org/10.1016/j.ocecoaman.2022.106323.
- Chen, X., Weng, C., Du, X., et al., 2023. Prediction of the rate of penetration in offshore large-scale cluster extended reach wells drilling based on machine learning and big-data techniques. Ocean Eng. 285, 115404. https://doi.org/10.1016/j.oceaneng.2023.115404.
- Evangelidis, A., Kugiumtzis, D., 2023. Adaptive decomposition of multicomponent signals and estimation of phase synchronization. IEEE Trans. Signal Process. 71, 1586–1598. https://doi.org/10.1109/TSP.2023.3271023.
- Fan, Y., Pang, Y., Jin, Y., et al., 2025. Integration of image recognition and expert system for real-time wellbore stability analysis. Adv. Geo-Energy Res 15 (2), 158–171. https://doi.org/10.46690/ager.2025.02.07.
- Gamal, H., Alsaihati, A., Ziadat, W., Mahmoud, A.A., Elkatatny, S., 2022. Ensemble Machine Learning Model for Predicting Rock Drillability Rate for Composite Lithology. The ADIPEC. Abu Dhabi. UAE. https://doi.org/10.2118/211779-MS.
- Gan, C., Wang, X., Wang, L.Z., et al., 2023. Multi-source information fusion-based dynamic model for online prediction of rate of penetration (ROP) in drilling process. Geoenergy Sci. Eng. 230, 212187. https://doi.org/10.1016/ i.geoen.2023.212187.
- Gao, Y., Chen, M., Jiang, H., 2021. Influence of unconnected pores on effective stress in porous geomaterials: theory and case study in unconventional oil and gas reservoirs. J. Nat. Gas Sci. Eng. 88, 103787. https://doi.org/10.1016/ j.jngse.2020.103787.
- Gong, Q., Xu, H., Lu, J., et al., 2022. Rock mass characteristics model for TBM penetration rate prediction— an updated version. Int. J. Rock Mech. Min. Sci. 149, 104993. https://doi.org/10.1016/j.ijrmms.2021.104993.
- Guo, J.X., Qian, J.X., Yan, A.X., et al., 2023. Noise reduction method for submarine cable vibration signal based on VMD and arrangement entropy. Opt. Commun. Tech. 48 (2), 84–89. https://doi.org/10.13921/j.cnki.issn1002-5561.2024.02.015.
- Hareland, G., Wu, A., Rashidi, B., 2010. A New Drilling Rate Model for Tri-cone Bits and Its Application to Predict Rock Compressive Strength. The 44th U.S. Rock Mechanics Symposium and 5th U.S.-Canada Rock Mechanics Symposium Salt Lake City, Utah. ARMA 10-206.
- He, K., Zhang, X., Ren, S., Sun, J., 2015. Deep Residual Learning for Image Recognition. 2016 IEEE Conference on Computer Vision and Pattern Recognition (CVPR), pp. 770–778. https://doi.org/10.1109/CVPR.2016.90.
- Hossain, M.A., Gray, E.M., Islam, M.R., et al., 2023. Optimized forecasting model to improve the accuracy of very short-term wind power prediction. IEEE Trans. Ind. Inf. 19, 10145–10159. https://doi.org/10.1109/TII.2022.3230726.
- Huang, N.E., Shen, Z., Long, S.R., et al., 1998. The empirical mode decomposition and the Hilbert spectrum for nonlinear and non-stationary time series analysis.

- Proc. Roy. Soc. Lond.: Math. Phys. Eng. Sci. 454, 903–995. https://doi.org/10.1098/rspa.1998.0193.
- Husam, H.A., Abo, T.A., Shari, D.N., 2021. Data-driven recurrent neural network model to predict the rate of penetration. Upstream. Oil. Gas. Tec. 7, 100047. https://doi.org/10.1016/j.upstre.2021.100047.
- Jiang, C., 2016. Research on Adaptive Fault Feature Extraction of Impulse Signal Based on EEMD and MED. PhD Thesis, Shanghai University.
- Li, D., Zhao, W., Hu, J., et al., 2023. A long-term water quality prediction model for marine ranch based on time-graph convolutional neural network. Ecol. Indic. 154, 110782. https://doi.org/10.1016/j.ecolind.2023.110782.
- Li, Q., Qu, F.T., He, J.B., et al., 2021. Rate of penetration for drilling prediction model based on PSO-BP. Sci. Technol. Eng. 21 (19), 7984–7990.
- Liu, J.B., Wei, H.S., Zhao, J.F., et al., 2015. A new 3D ROP equation considering the rotary speed of bit. Petroleum Drilling Techniques 43 (1), 56–61. https://doi.org/10.11911/syztjs.201501009 (in Chinese).
- Liu, Y., Zhang, F.Q., Yang, S.P., et al., 2023. Self-attention mechanism for dynamic multi-step ROP prediction under continuous learning structure. Geoenergy Sci. Eng. 229, 212083. https://doi.org/10.1016/j.geoen.2023.212083.
- Maurer, W.C., 1962. The "perfect-cleaning" theory of rotary drilling. J. Petrol. Technol. 14 (11), 1270–1274. https://doi.org/10.2118/408-PA.
- Melvin, B.D., Kim, K.Y., Shin, H.S., et al., 2019. Predicting rate of penetration during drilling of deep geothermal well in Korea using artificial neural networks and real-time data collection. J. Nat. Gas Sci. Eng. 67, 225–232. https://doi.org/ 10.1016/j.ingse.2019.05.004.
- Musluoglu, C.A., Bertrand, A., 2023. A unified algorithmic framework for distributed adaptive signal and feature fusion problems-part I: algorithm derivation. IEEE Trans. Signal Process. 71, 1863—1878. https://doi.org/10.1109/TSP.2023.3275272.
- Nadirgil, O., 2023. Carbon price prediction using multiple hybrid machine learning models optimized by genetic algorithm. J. Environ. Manag. 342, 118061. https:// doi.org/10.1016/j.jenvman.2023.118061.
- Osman, H., Ali, A., Mahmoud, A.A., et al., 2021. Estimation of the rate of penetration while horizontally drilling carbonate formation using randomforest. J. Energy Resour. Technol. 143, 093003. https://doi.org/10.1115/1.4050778.
- Ouyang, H.B., Huang, K., Yan, H.J., 2020. Prediction of financial time series based on LSTM neural network. Chin. J. Manag. Sci. 28 (4), 27–35. https://doi.org/10.16381/j.cnki.issn1003-207x.2020.04.003 (in Chinese).
- Oyedere, M., Gray, K., 2020. ROP and TOB optimization using machine learning classification algorithms. J. Nat. Gas Sci. Eng. 77, 103230. https://doi.org/10.1016/j.jngse.2020.103230.
- Pang, H.W., Meng, H., Wang, H.Q., et al., 2022. Lost circulation prediction based on machine learning. J. Petrol. Sci. Eng. 208, 109364. https://doi.org/10.1016/ i.petrol.2021.109364.
- Pei, Z.J., Song, X.Z., Wang, H.T., et al., 2024. Interpretation and characterization of rate of penetration intelligent prediction model. Pet. Sci. 21 (1), 582–596. https://doi.org/10.1016/j.petsci.2023.10.011.
- Peng, Z.Y., Peng, S., Fu, L.D., et al., 2020. A novel deep learning ensemble model with data denoising for short-term wind speed forecasting. Energy Convers. Manag. 207, 112524. https://doi.org/10.1016/j.enconman.2020.112524.
- Qiu, Y., Ma, T., Peng, N.ian, Liu, Y., et al., 2023. Wellbore stability analysis of inclined wells in transversely isotropic formations accounting for hydraulic-mechanical coupling. Geoenergy Sci. Eng. 224, 211615. https://doi.org/10.1016/j.geoen.2023.211615.
- Song, C., Wang, T., Chen, X.H., et al., 2023. Ensemble framework for daily carbon dioxide emissions forecasting based on the signal decompositionreconstruction model. Appl. Energy 345, 121330. https://doi.org/10.1016/ j.apenergy.2023.121330.
- Sun, S.L., Wei, Y.J., Wang, Y.S., 2022. Exchange rates forecasting method with decomposition-clustering-ensemble learning approach. Syst. Eng. -Theory & Practice 42 (3), 664–677. https://doi.org/10.12011/SETP2019-1550.
- Valverde, G., Quesada, D., Larrañaga, P., et al., 2023. Causal reinforcement learning based on Bayesian networks applied to industrial settings. Eng. Appl. Artif. Intell. 125, 106657. https://doi.org/10.1016/j.engappai.2023.106657.
- Wang, H.M., Liu, Y.Q., Liao, Y.Y., 2020. Fault diagnosis method for rolling bearings based on fast spectral kurtosis and orthogonal matching pursuit algorithm. J. Vib. Shock 39 (19), 78–83+100. https://doi.org/10.13465/j.cnki.jvs.2020.19.012.
- Wang, L., Zhou, Z., Wei, J., et al., 2022a. Learning causal Bayesian networks based on causality analysis for classification. Eng. Appl. Artif. Intell. 114, 105212. https:// doi.org/10.1016/j.engappai.2022.105212.
- Wang, R.Z., Zhang, X.S., Wang, M.H., 2022b. Agricultural product price prediction based on signal decomposition and deep learning. Trans. Chin. Soc. Agric. Eng. 38 (24), 256–267. https://doi.org/10.11975/j.issn.1002-6819.2022.24.028.
- Wang, Z.C., Chen, L.R., Chen, H.Y., et al., 2023. Monthly ship price forecasting based on multivariate variational mode decomposition. Eng. Appl. Artif. Intell. 125, 106698. https://doi.org/10.1016/j.engappai.2023.106698.
- Wu, Z.H., Huang, N.E., 2009. Ensemble empirical mode decomposition: a noise-assisted data analysis method. Adv. Adapt. Data Anal. 1 (1), 1–41. https://doi.org/10.1142/S1793536909000047.
- Yan, J., Li, C., Ma, D., et al., 2024. Dynamic and static feature identification method of complex buried hill reservoirs in Bohai and its application. Petroleum. Reserv. Eval. and Development 14 (2), 308–316. https://doi.org/10.13809/j.cnki.cn32-1825/te 2024.02.016
- Yang, W., Xia, K., Fan, S., 2023. Oil logging reservoir recognition based on TCN and SA-BiLSTM deep learning method. Eng. Appl. Artif. Intell. 121, 105950. https://doi.org/10.1016/j.engappai.2023.105950.

- Zhang, S., Luo, J., Wang, S., et al., 2023. Oil price forecasting: a hybrid GRU neural network based on decomposition—reconstruction methods. Expert Syst. Appl.
- 218, 119617. https://doi.org/10.1016/j.eswa.2023.119617. Zhang, Y., Zhao, Y., Pan, G., et al., 2020. Wind speed interval prediction based on Lorenz disturbance distribution. IEEE Trans. Sustain. Energy 11, 807–816.
- https://doi.org/10.1109/TSTE.2019.2907699.

  Zheng, Z., Wang, Z.J., Zhu, Y., et al., 2019. Feature extraction method for hydraulic pump fault signal based on improved empirical wavelet transform. Processes 7 (11), 824–835. https://doi.org/10.3390/pr7110824.